AD-A250 135
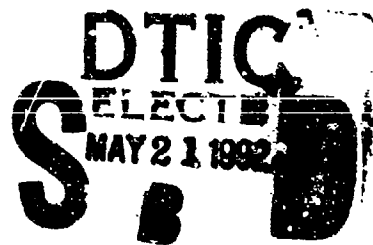
A DETECTOR FOR STATIONARY GAS BUBBLES:
FEASIBILITY STUDIES

G. Albin
P. Massell
W. Mints
J. Himm

DTIC
SELECTED
MAY 21 1992
S B D

92-13427

92 5 19 095

NOTICES

The opinions and assertions contained herein are the private ones of the writer and are not to be construed as official or reflecting the views of the naval service at large.

When U. S. Government drawings, specifications, or other data are used for any purpose other than a definitely related Government procurement operation, the Government thereby incurs no responsibility nor any obligation whatsoever, and the fact that the Government may have formulated, furnished or in any way supplied the said drawings, specifications, or other data is not to be regarded by implication or otherwise, as in any manner licensing the holder or any other person or corporation, or conveying any rights or permission to manufacture, use, or sell any patented invention that may in any way be related thereto.

Please do not request copies of this report from the Naval Medical Research Institute. Additional copies may be purchased from:

Federal Government agencies and their contractors registered with the Defense Technical Information Center should direct requests for copies of this report to:

TECHNICAL REVIEW AND APPROVAL

NMRI 92-25

The experiments reported herein were conducted according to the principles set forth in the current edition of the "Guide for the Care and Use of Laboratory Animals," Institute of Laboratory Animal Resources, National Research Council.

This technical report has been reviewed by the NMRI scientific and public affairs staff and is approved for publication. It is releasable to the National Technical Information Service where it will be available to the general public, including foreign nations.

LARRY W. LAUGHLIN
CAPT, MC, USN
Commanding Officer
Naval Medical Research Institute

REPORT DOCUMENTATION PAGE

1a. REPORT SECURITY CLASSIFICATION	1b. RESTRICTIVE MARKINGS
UNCL	

2a. SECURITY CLASSIFICATION AUTHORITY	3. DISTRIBUTION / AVAILABILITY OF REPORT
2b. DECLASSIFICATION / DOWNGRADING SCHEDULE	Approved for public release; distribution is unlimited

4. PERFORMING ORGANIZATION REPORT NUMBER(S)	5. MONITORING ORGANIZATION REPORT NUMBER(S)
NMRI 92-25	

6a. NAME OF PERFORMING ORGANIZATION	6b. OFFICE SYMBOL (If applicable)	7a. NAME OF MONITORING ORGANIZATION
Naval Medical Research Institute		Naval Medical Command

6c. ADDRESS (City, State, and ZIP Code)	7b. ADDRESS (City, State, and ZIP Code)
8901 Wisconsin Avenue Bethesda, MD 20814-5055	Department of the Navy Washington, DC 20372-5120

8a. NAME OF FUNDING/SPONSORING ORGANIZATION Naval Medical Research & Development Command	8b. OFFICE SYMBOL (If applicable)	9. PROCUREMENT INSTRUMENT IDENTIFICATION NUMBER

8c. ADDRESS (City, State, and ZIP Code)	10. SOURCE OF FUNDING NUMBERS			
8901 Wisconsin Avenue Bethesda, MD 20814-5044	PROGRAM ELEMENT NO.	PROJECT NO.	TASK NO.	WORK UNIT ACCESSION NO.
	62233N	MM33P30	.004	1050

11. TITLE (Include Security Classification)

(U) A DETECTOR FOR STATIONARY GAS BUBBLES: FEASIBILITY STUDIES

12. PERSONAL AUTHOR(S)
G. Albin, P. Massell, W. Mints, and J. Himm

13a. TYPE OF REPORT	13b. TIME COVERED	14. DATE OF REPORT (Year, Month, Day)	15. PAGE COUNT
Technical Report	FROM 8/89 TO 1/91	1992 April	94

16. SUPPLEMENTARY NOTATION

17.	COSATI CODES		18. SUBJECT TERMS (Continue on reverse if necessary and identify by block number)
FIELD	GROUP	SUB-GROUP	bubble detection, ultrasound, Doppler, bubble oscillation, noninvasive testing, decompression sickness

19. ABSTRACT (Continue on reverse if necessary and identify by block number)

Work progresses on developing operating procedures for a system intended to detect stationary gas bubbles of diameters 0.9 to 6 μm using ultrasonic interrogation. The original system has been redesigned and is now configured for menu-driven remote control from a PC. Signal averaging and subtraction of measured background noise are available for maximizing the signal/noise (S/N) ratio. The output signal is now a spectrum consisting of the [amplitude of the 2nd harmonic distortion component of the output signal] versus the [frequency of the input signal]. For well-characterized physical systems, it should be possible to deduce bubble sizes from this spectrum. Calibration standards, consisting of stable bubbles in the 0.9 to 6 μm size range, have proven difficult to prepare. The reason for this difficulty is that size changes in such small spherical bubbles usually are fast relative to the measurement time, s has been studied using a mathematical simulation. Nonetheless, work will now proceed without calibration, using less well-defined bubble populations to test the

20. DISTRIBUTION / AVAILABILITY OF ABSTRACT	21. ABSTRACT SECURITY CLASSIFICATION
☒ UNCLASSIFIED/UNLIMITED ☐ SAME AS RPT. ☐ DTIC USERS	Unclassified

22a. NAME OF RESPONSIBLE INDIVIDUAL	22b. TELEPHONE (Include Area Code)	22c. OFFICE SYMBOL
Regina E. Hunt, Command Editor	(202) 295-0198	SD/RSD/NMRI

DD FORM 1473, 84 MAR   83 APR edition may be used until exhausted   SECURITY CLASSIFICATION OF THIS PAGE
All other editions are obsolete   UNCLASSIFIED

system's ability to detect bubbles categorically (i.e., "bubbles" or "no bubbles"). To predict the S/N ratio for single bubbles in water, we have been used mathematical simulations of vibrating bubbles in conjunction with measurements of the system noise. Solutions have been obtained for the equation of motion outside of a bubble vibrating in a liquid or in an elastic solid using both an approximate analytic technique (namely, the Method of Perturbation) and a more accurate numerical technique (a Galerkin method).

TABLE OF CONTENTS

LIST OF FIGURES

Accession For

NTIS GRA&I	☑
DTIC TAB	☐
Unannounced	☐
Justification	

By

Distribution/

Availability Codes

| Dist | Avail and/or Special |
| A-1 | |

v

ACKNOWLEDGEMENTS

I. INTRODUCTION

Symptoms of decompression sickness (DCS) typically are assumed to result from the formation of gas bubbles in blood or extravascular tissue. Information on extravascular bubbles has been severely limited by the lack of any noninvasive method of observing them.

In a previous report (NMRI Technical Report 91-39, <u>Basic Operation of a Detector for Stationary Gas Bubbles</u>[1]), we discussed a system constructed at the Jet Propulsion Laboratory (JPL) that uses ultrasound to detect stationary gas bubbles. We call the system the 'JPL swept frequency bubble detector', or simply the 'bubble detector'. The bubble detector can, in principle, enable the quantitative measurement of the sizes and numbers of stationary extravascular bubbles. Its theory of operation depends on these facts: 1) gas bubbles are the softest objects in tissue, and consequently undergo the largest deformations when vibrating in a sound field, 2) although vibrations are linear at sufficiently small deformations, they become increasingly nonlinear at larger deformations[2], and 3) nonlinear vibrations contain harmonics and subharmonics -- that is, the vibrations contain multiple frequency components even when the driving signal is monotonal. In theory therefore, when tissue is driven to vibration by externally applied sound of moderate amplitude, any harmonics or subharmonics in the sound backscattered from the tissue should be attributable to gas bubbles rather than to stiffer objects. More specifically, the bubble detector is designed to exploit the 'second harmonic' component of the energy backscattered by vibrating bubbles (the component having the frequency twice that of the driving signal).

1

A brief description of the bubble detector is offered here. The reader should look to reference 1 for a more comprehensive discussion.

The bubble detector uses a transmitting pressure transducer to broadcast a swept-frequency sound pressure field onto a target and a receiving pressure transducer to detect the sound backscattered from the target. It then filters out all frequency components in the output signal except for either the second harmonic or the 'fundamental' (the component having the same frequency as the driving signal), as desired. The filtered signal is then processed to give two types of conditioned output signals. In the 'range' mode the system produces an amplitude spectrum (i.e., a plot of amplitude versus frequency) in which the independent variable is the difference in frequency between the transmitted and received signals. This frequency offset is proportional to the time delay between sound transmission and reception of the backscattered sound from the target. The distance from the transducer head to the target is calculated from the corresponding frequency offset.

In the 'frequency response' ('FRC') mode, the system generates a spectrum in which the independent variable is the frequency of the transmitted signal (referred to hence as the 'forcing frequency' or 'driving frequency') and the dependent variable is the amplitude of the backscattered signal from any targets that are at a certain preselected distance from the transducer head. This output shows the 'frequency response' of the system consisting of both the bubble and the bubble detector; that is, it shows how strongly the system responds to its input as a function of the input frequency. In theory, this information should enable one to assay a bubble population: the location of a

2

resonance peak in the spectrum depends on the bubble diameter and the peak size is proportional to the number of bubbles at that diameter. The transducers supplied by JPL operate over a frequency range of ~1-7 Mhz, which encompasses the main resonance frequencies of bubbles in H_2O of roughly 0.9-6.0 microns diameter, so we can reasonably expect to be able to identify bubbles in this size range.[*]

The first technical report in this series dealt with the basic operation of the bubble detector. As it was being written, the following goals had been achieved:

1) A computer routine that uses an approximate, analytic solution to the differential equations describing a vibrating bubble to compute the amplitude of the second harmonic component of the sound radiated from a bubble *in a viscous liquid* as a function of the frequency of incident sound.

2) A protocol for preparing calibration standards consisting of known bubble populations by trapping gas bubbles in transparent hydrogels and determining the sizes and numbers of bubbles in the gels microscopically.

3) Indications that, through conducting preliminary, semi-quantitative experiments with bubbles in hydrogels, the signal/noise ratio of the system as delivered was unacceptably low.

We report here on our continuation of bubble detection studies. The work generally has been directed toward redesigning the original system to remove shortcomings that

---

[*] In NMRI Technical Report 91-39, it was stated that the transducers operated over the frequency range 0.2-5 MHz, encompassing the main resonance frequencies of bubbles of ~1-20 μm diameter. This statement was erroneous. By direct measurement, the frequency response of the bubble detector system as a whole is reasonably strong over the range of ~1-7 MHz; the manufacturer of the transducers states that the transducers were *designed* for operation over the 2-10 MHz range.

severely limited its utility, and determining whether the output signal-to-noise (S/N) ratio is high enough to enable quantitative analysis of the data for bubbles up to 6 μm diameter. We eventually had to evaluate the S/N ratio using theory rather than empiricism because we have found bubbles this small to be too short-lived *in vitro* to permit their examination using both the bubble detector and a suitable microscope (the latter being used to establish bubble size). In fact, the theory discussed in Section V on the stability of bubble populations in a closed system suggests that it is impractical to extend the lifetimes of such small bubbles to sufficient length for our purposes in a system of constant surface tension.

The following new goals have been achieved and will be discussed in this report:

1) Replacing the analogue AM tuner, which was provided with the original system for demodulating AM signals, with a commercially available signal analyzer capable of digital demodulation. This improves the system's S/N ratio somewhat. More importantly, the signal analyzer has been interfaced with a PC upon which digitized data can be stored, which makes the numerical data available to us for the first time.

2) Exploring strategies for preparing suitable calibration standards consisting of quasi-stable bubbles trapped in polymer gels.

3) Elucidating whether small spherical bubbles can be stabilized (for the purpose of producing calibrants) without invoking complicated mechanisms involving variable surface tension or variable permeability at the bubble surface.

4

Developing and exploring a mathematical simulation of the growth and shrinkage of bubbles in a closed system with finite surface tension.

4) Developing an approximate, analytic solution to the differential equations describing a vibrating bubble in an *elastic solid* and coding it as computer routines. This approach uses linearized elastic theory (valid for small deformations) to model the elastic stress associated with oscillations and nonlinear elastic theory to describe the potentially large elastic stress present at the bubble wall at rest.

5) Writing into computer code a more accurate, numerical solution to the differential equations describing a vibrating bubble in a viscous liquid and in an elastic solid.

6) Measuring system noise has been measured.

7) Estimating the S/N ratio cf the system for single bubbles in the size range for which the system was designed by using the system noise measurements and the predictions of the mathematical models.

The mathematical simulations mentioned in items 4 and 5 will allow computation of the amplitude of the 2nd harmonic component of the sound radiated from a bubble as a function of the frequency of incident sound.

The analytic expressions noted in item 4 can be evaluated quickly enough on even a modest computer to make them useful for deducing the sizes and numbers of bubbles in a sample containing an unknown bubble population using an iterative curve-fitting/parameter estimation approach, as follows:

We will fit a curve to the voltage amplitude versus driving frequency data provided by the bubble detector in its 'frequency response' mode, with the values of bubble diameter and bubble number taken as adjustable parameters to be optimized in the curve-fitting routine. The data-fitting will consist of minimizing the sum of squares of error (SSE) using a Marquardt least-squares algorithm.[3] The SSE is a measure of the goodness-of-fit of the model to the data. The independent variable is the driving frequency, the dependent variable is the voltage amplitude, and for an unknown target sample the parameters to be estimated are bubble radius and bubble number. The Marquardt algorithm is an iterative routine that systematically adjusts the values of each unknown parameter 'B' based on the value of $\partial(SSE)/\partial B$ in the current iteration.

The numerical solutions mentioned in item 5 are much more CPU-intensive than the analytic expressions, but presumably more accurate, and will be used to evaluate the accuracy of the analytic solutions. There is a lack of experimental verification of any theory's predictions regarding the 2nd harmonic component of bubble oscillations.

The simulation of bubble dynamics (listed as item 3 above) indicates that quasi-stable bubbles of diameters $<100\,\mu$m cannot be obtained in a system of constant surface tension. Our own efforts to obtain small, quasi-stable bubbles (mentioned above in item 2) produced no results to the contrary: we were unsuccessful in attempts to prepare suitable calibration standards containing bubbles in the size range of interest.

The mathematical descriptions of bubble behavior from items 4 and 5 enable us to estimate the output voltage amplitude that should be observed for a $6\,\mu$m bubble driven

at its main resonance frequency. (This is the strongest output signal that would be observed for any bubble of ≤6 μm diameter at any driving frequency.) By comparison with the measured noise floor, we have estimated the S/N ratio. The result of this estimate casts some doubt on the practicality of quantitatively studying individual bubbles in the 0.9-6 μm range. The proper course of action may be to study larger bubbles, thus increasing the S/N ratio without improving any electronic components. This necessitates the purchase of pressure transducers designed to operate over a lower frequency range than the pair originally supplied. The size range of stationary bubbles that are most relevant to DCS is unknown, so there is no reason to insist upon studying bubbles of any particular size range so long as the size is physiologically plausible.

II. ADDING DIGITAL AM SIGNAL DEMODULATION TO THE SYSTEM

A. Impetus for adding digital AM demodulation

As noted in the Introduction, the bubble detector has two operating modes: the 'range' mode, in which the signal is Fourier-transformed to give information on bubble location, and the 'frequency response', or FRC mode, in which the signal is demodulated to give information about the sizes and numbers of bubbles.

For the frequency response mode, the bubble detector (as delivered by JPL) included a section for analogue demodulation of amplitude modulated (AM) signals; i.e. an AM tuner. The tuner consisted of a local oscillator, a mixer, and a low-pass filter. It was noted in reference 1 that the tuner section was a significant noise source. It was noted also that the bubble detector's output signal was analog and that no means had been provided for digitizing or recording the output, preventing meaningful data analysis. In addition, the output was not an amplitude spectrum, as expected from a system intended to function as a spectrum analyzer, but rather was the sum of waveforms of various frequencies, each waveform associated with one of the acoustic targets in front of the pressure transducers. This sort of output does not lend itself readily to objective analysis.

In order for the bubble detector to have potential as a research tool, the problems noted above must be overcome. Replacing the AM tuner with a digital signal analyzer capable of AM signal demodulation can solve all three of them. Digital signal processing does not contribute appreciably to noise, commercially available digital

8

processors normally can be interfaced with computers on which data can be stored and processed, and we will see that the output of an AM demodulator for this system is an amplitude spectrum whose relationship with the physical system under study is easy to conceptualize.

B. Hardware

Demodulating an AM signal is equivalent to recovering the amplitude versus time information; for this system the input frequency is a linear function of time, and therefore the demodulated signal is equivalent to a spectrum of amplitude versus forcing frequency. A Hewlett-Packard 3561A signal analyzer was chosen for the task. This machine cannot actually demodulate signals, but it can separate a signal into its real and imaginary parts. These are captured and sent to a PC, on which the amplitude is computed at each time point simply by taking the square root of the sum of the squares of the real and imaginary parts. The HP 3561A simultaneously carries out a fast Fourier transformation (FFT) on the signal, thus performing the range mode task at the same time as it handles the FRC mode function.

C. Software

The Appendix contains the HP Basic program used to remotely control the HP 3561A and the HP 3325A signal generator from an IBM-compatible PC in which a Hewlett-Packard Basic Language Processor card has been installed. The program runs measurement 'cycles', pausing between cycles for a user-selectable length of time. During each cycle the program 1) prompts the bubble detector to make a series of measurements, 2) extracts the raw output from these measurements from the signal

9

analyzer, 3) converts them to amplitude-versus-forcing frequency spectra for the FRC output, 4) averages the spectra from multiple measurements (i.e., uses 'signal averaging') to minimize white noise, 5) subtracts from the spectrum a signal-averaged "background" measurement taken at the beginning of the experiment when bubbles are absent, 6) stores the result to hard disk, and 7) plots the result on a Hewlett-Packard printer. The user chooses an appropriate target for the background measurement. For example, if bubbles are to be formed in an acoustical target during the experiment, one chooses as background the target itself before the introduction of bubbles.

Simultaneously, the 3561A also performs an FFT on the data for the range mode output. The result is transferred to the PC along with the FRC spectrum and is then printed. A few examples of the final outputs from both the FRC and range modes are shown in the following section.

The program allows the user to select values of the following operating parameters:

1) frequency range of the frequency sweep (i.e., the start and stop frequencies)

2) sweep time

3) voltage amplitude generated by the 3325A signal generator

4) analyzer frequency 'span' (explained below)

5) 'start frequency' for the analyzer (explained below)

6) number of sweeps to be averaged together during the cycle in which the background noise is measured

7) number of sweeps to be averaged together during each cycle in which a signal is measured

10

8) how long to pause between cycles

D. On the selection of operating parameters

We will now consider the analyzer's start frequency, its frequency span, and how to chose each correctly. The HP 3561A analyzer captures all signals having frequencies between the start frequency and the sum of [start frequency + frequency span]. Higher and lower frequencies are filtered out. Therefore, the span is the bandwidth of the captured signals. The user wants the signal analyzer to capture the output signal only while the signal generator is performing a frequency sweep. The synchrony between these two instruments is realized by having the analyzer triggered by the generator at the *start* of the sweep. The analyzer also should *stop* capturing data at the same time as the sweep is completed. In other words, the 'time record' captured by the analyzer should be the same duration as the sweep time. The correct choice of span ensures this, as we discuss now.

The HP 3561A analyzer always collects $2^{10} = 1024$ digital samples per time record. The sample rate is thereby determined:

$$\text{sample rate} \ = \ (1024 \text{ samples})/(\text{length of time record}) \qquad [1]$$

The sample rate is always $2.56 \cdot$ span. Because the time record length should equal the sweep time, we see by inspection that

$$\text{span} \ = \ 400/(\text{sweep time}) \qquad [2]$$

11

where the span is in Hz and the sweep time is in seconds. The program automatically selects the correct span for a given sweep time, and vice-versa. One must manually select the start frequency such that signals of interest have frequencies greater than the start frequency and less than [start frequency + span].

As an illustration, the frequency of the signal received from an acoustical target is given by

$$f_{signal} = \frac{2 \ (bandwidth \ of \ sweep, \ Hz) \cdot (distance, \ cm)}{(sweep \ time, \ sec) \cdot (velocity \ of \ sound, \ \sim 1.5 \cdot 10^5 \ cm/sec \ in \ water)} \qquad [3]$$

where the 'distance' in the numerator is measured between the transducer head and the target[1]. For example, a 0.2-second sweep from 1 MHz to 7 MHz yields a signal of 1.3 kHz for a bubble located 3.25 cm from the transducers (the transducer head is shaped to optimize performance for a distance of roughly 3.25 cm). If we record a time record for a 0.2-second sweep, the frequency span will be 2 kHz (as shown in Equation [2]). We might set the start frequency at 1 kHz to capture all signals between 0.8 and 2.8 kHz, thus ensuring that the target associated with the 1.3 kHz signal is detected.

In the FRC mode any signals within the frequency span are lumped together in the conversion to amplitude, so that there is no resolution of frequencies for any signals that fall within the frequency span. Therefore, for the example given there is no frequency resolution in the FRC mode for signals ranging from 0.8 to 2.8 kHz. The most precise statement we could make about a bubble's location, based only on the information from

12

the FRC mode output, would be that its distance from the transducer head is between 2 cm and 7 cm.

Although the range mode *does* give us the information necessary for deducing the distances of bubbles from the transducers, the presence of more than one bubble will lead to ambiguity about which peak in the range mode spectrum corresponds to which peak(s) in the FRC mode. In other words, associating bubble sizes with bubble locations may be a hit-or-miss procedure.

One further point: whereas there is a large DC noise component and also some noise at 60 Hz, the start frequency should be set no lower than a few hundred Hz so that these spurious components are digitally filtered out by the 3561A before further signal processing.

III. THE OUTPUT SIGNAL

In this section examples of the system's output signal will be shown and discussed for various acoustical targets. In all cases the amplitude of the 2nd harmonic component of the backscattered signal is plotted.

All measurements in this section were made under the following conditions:

sweep time = 0.2 sec
span = 2 kHz (therefore, time record length = 0.2 sec)
sweep start frequency = 2 MHz
sweep stop frequency = 10 MHz
windowing = flattop
signal averaging: 15 time records averaged
target distance ~ 3.25 cm

The frequency range is that over which the transducer pair was *designed* to operate, not necessarily the optimal range. The measurements were made using signal averaging over 15 frequency sweeps. It was observed that the averaged signal changes negligibly after ~5 averages, and therefore after 15 averages the uncorrelated noise has been minimized, so that 15 averages yields the same result as would averaging indefinitely.

Figures 1a and 1b show measurements made when the transmitted signal is reflected from a slab of Wall-Gone sound absorber. The upper plots are the FRC mode outputs and the lower ones are the range mode outputs (explained in the Introduction). The FRC portion of Figure 1a is called a 'background' measurement and the FRC portion of Figure 1b is a measurement of [signal + background - background]. There is no

BACKGROUND @ 14:04:59   31 May 1991

300 uV

Voltage — Amplitude

0 uV

-300 uV

2   10

Forcing Frequency (MHz)

POSITIVE AREA IS   +641.684 microvolts-MHz
NEGATIVE AREA IS   0.000 microvolts-MHz

BACKGROUND TRACE

100 uV

Voltage — Amplitude

0 uV

1   3

Offset Frequency (kHz)
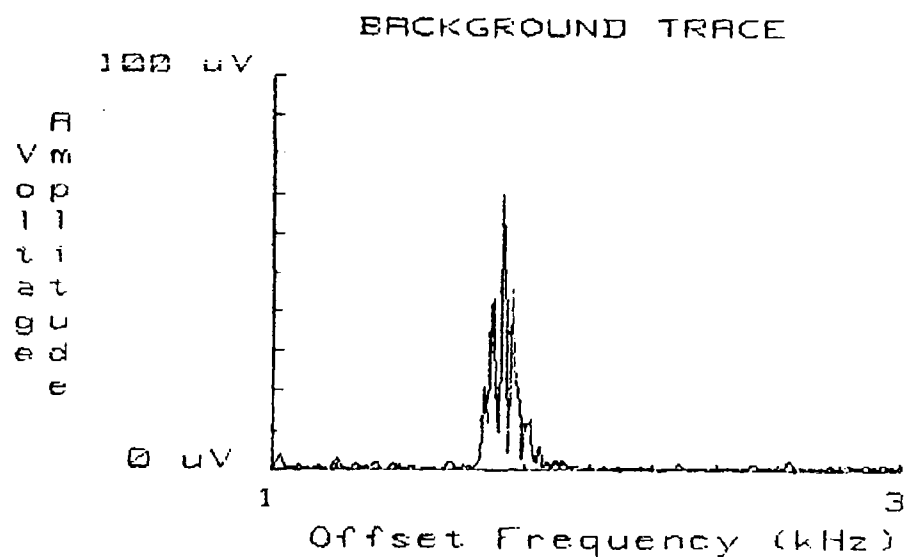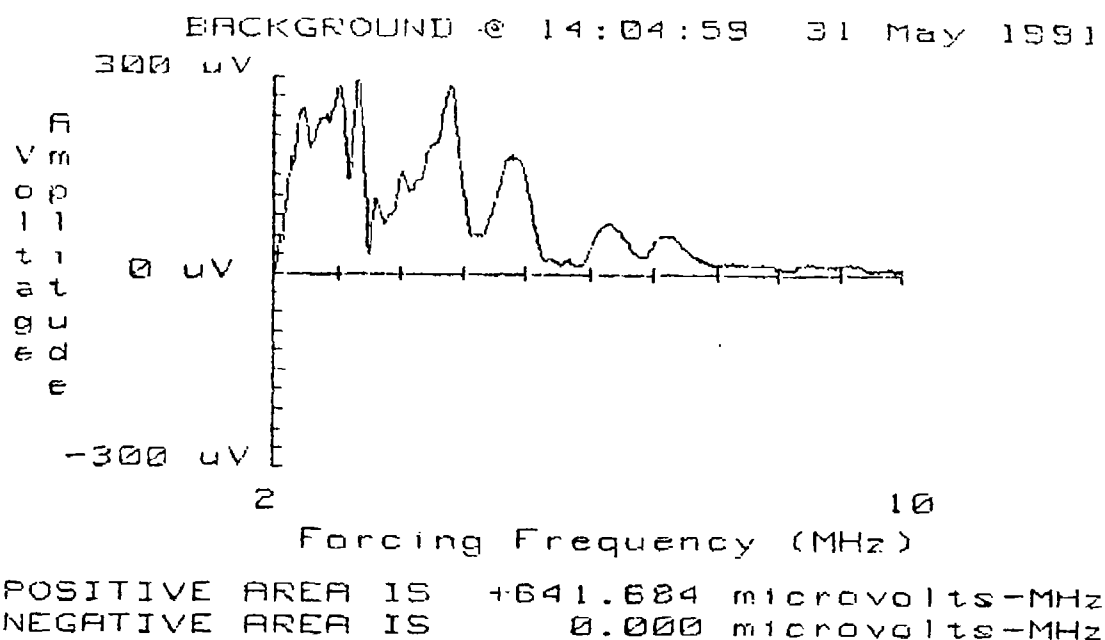
FIGURE 1A: OUTPUT SIGNAL; ACOUSTICAL TARGET IS WALL-GONE; BACKGROUND MEASUREMENT.

15

SIGNAL @ 14:17:43

100 uV

A
V m
o p
l l
t i
a t
g u
e d
e

0 uV

-100 uV

2   10

Forcing Frequency (MHz)

POSITIVE AREA IS   +5.571 microvolts-MHz
NEGATIVE AREA IS   -5.162 microvolts-MHz

SIGNAL TRACE

100 uV

A
V m
o p
l l
t i
a t
g u
e d
e

0 uV

1   3

Offset Frequency (kHz)
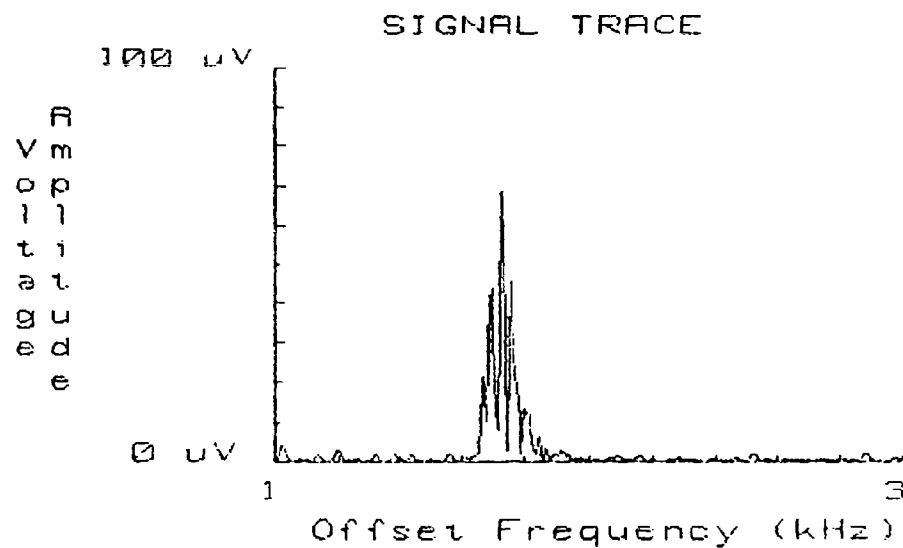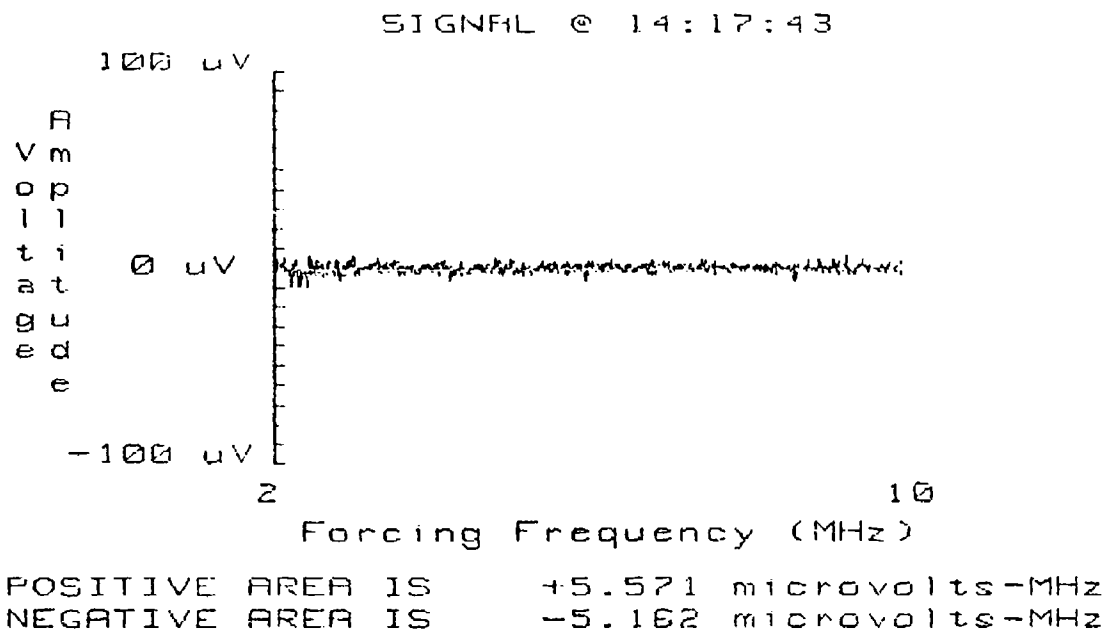
**FIGURE 1B: OUTPUT SIGNAL; ACOUSTICAL TARGET IS
WALL-GONE; SIGNAL MINUS BACKGROUND.**

16

background subtraction being performed on the range mode output. Because Figure 1b was obtained simply by repeating the background measurement, its FRC output should show nearly zero voltage, as it does. The time at which the signal was measured is recorded in the header of each plot.

In Figure 2, we see similar measurements made with a 3-mm-thick slab of polyacrylamide (PAAm) gel sitting on top of the Wall-Gone. There are no bubbles in the gel.

Under each FRC plot we record the "positive area" between the x-axis and the positive portion of the curve and the "negative area" between the x-axis and the negative portion of the curve, computed using trapezoidal integration. They are useful indices that quantify the results in an easily understood way.

Figures 1b and 2b demonstrate that subtracting an appropriate background can reduce the noise by at least an order of magnitude. It is seen that the residual after background subtraction is much greater with the PAAm target (Figure 2) than with the Wall-Gone. This observation has been reproduced in several additional measurements with both PAAm and Wall-Gone (not shown). Obviously, the backscattered signal changes appreciably from one measurement cycle to the next when replicate measurements are made with a PAAm gel. The reason for this change is not yet clear.

The lumpiness of the frequency responses seen in the background measurements in Figures 1 and 2 results from beating between two or more signals of similar frequencies. To understand this, consider that in the experiment of Figure 2 the bubble detector is receiving signals reflected from both the front and back surfaces of the

17

BACKGROUND @ 17:05:56   31 May 1991

1100 uV

A
V m
o p
l l
t i
a t
g u
e d
   e

0 uV

-1100 uV

2   10

Forcing Frequency (MHz)
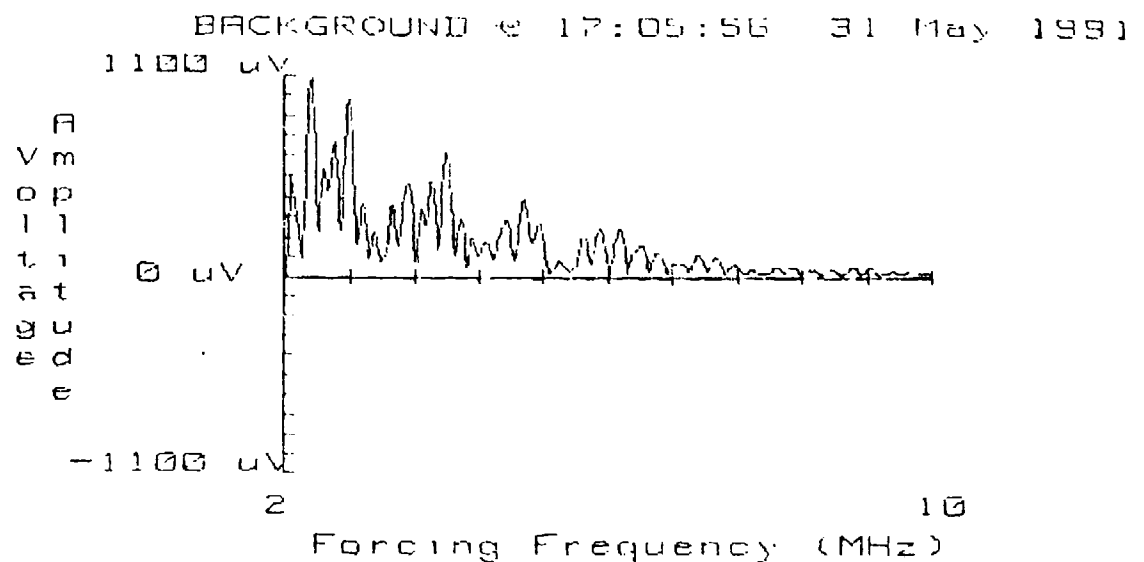
POSITIVE AREA IS +1402.211 microvolts-MHz
NEGATIVE AREA IS   0.000 microvolts-MHz

BACKGROUND TRACE

200 uV

A
V m
o p
l l
t i
a t
g u
e d
   e

0 uV

1   3

Offset Frequency (kHz)
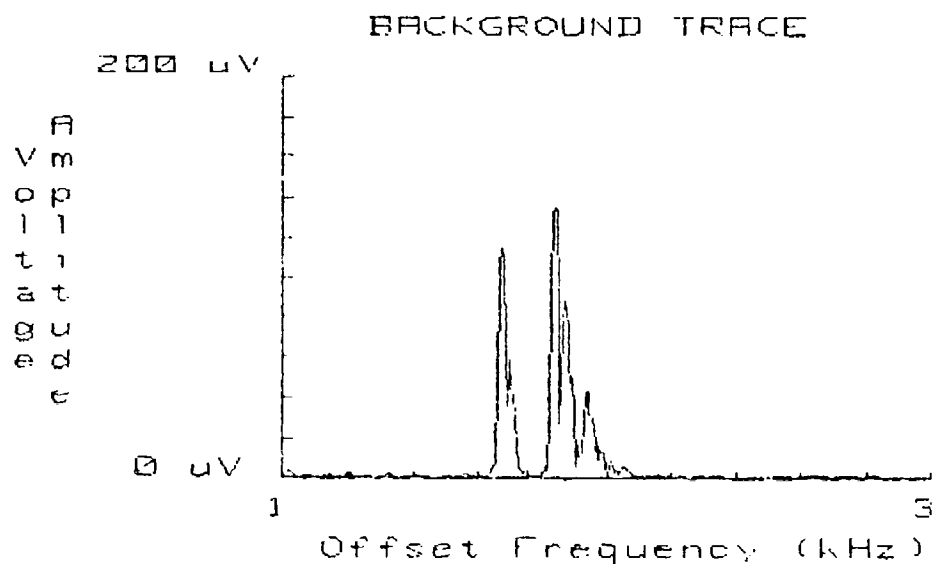
FIGURE 2A: OUTPUT SIGNAL; ACOUSTICAL TARGET IS
              A 3 MM-THICK PAAM GEL MOUNTED ON
              WALL-GONE; BACKGROUND MEASUREMENT.

18

SIGNAL @ 17:17:45

200 uV

A
V m
o p
l l
t i
a t
g u
e d
   e

0 uV

-200 uV

2   10

Forcing Frequency (MHz)

POSITIVE AREA IS   +114.138 microvolts-MHz
NEGATIVE AREA IS   -48.145 microvolts-MHz

SIGNAL TRACE

200 uV

A
V m
o p
l l
t i
a t
g u
e d
   e

0 uV

1   3

Offset Frequency (kHz)
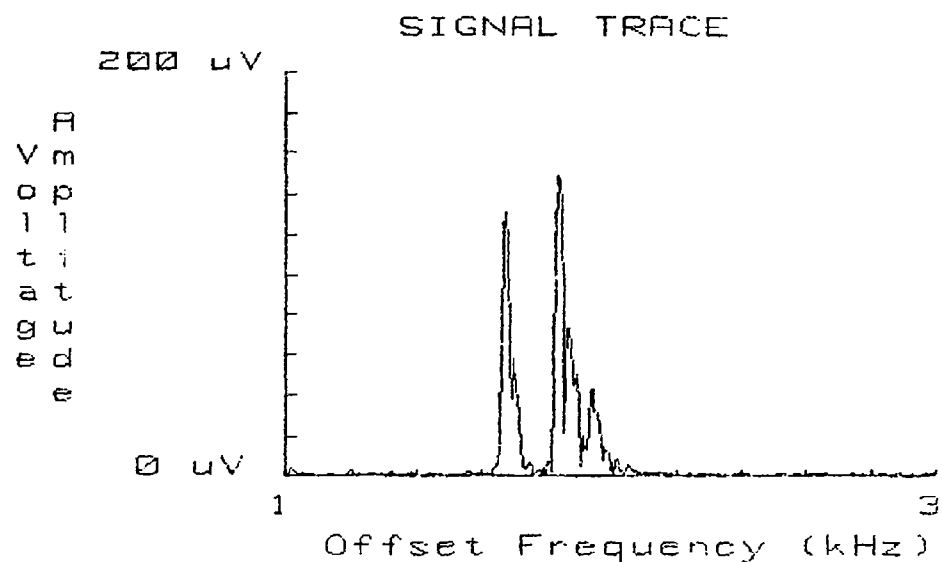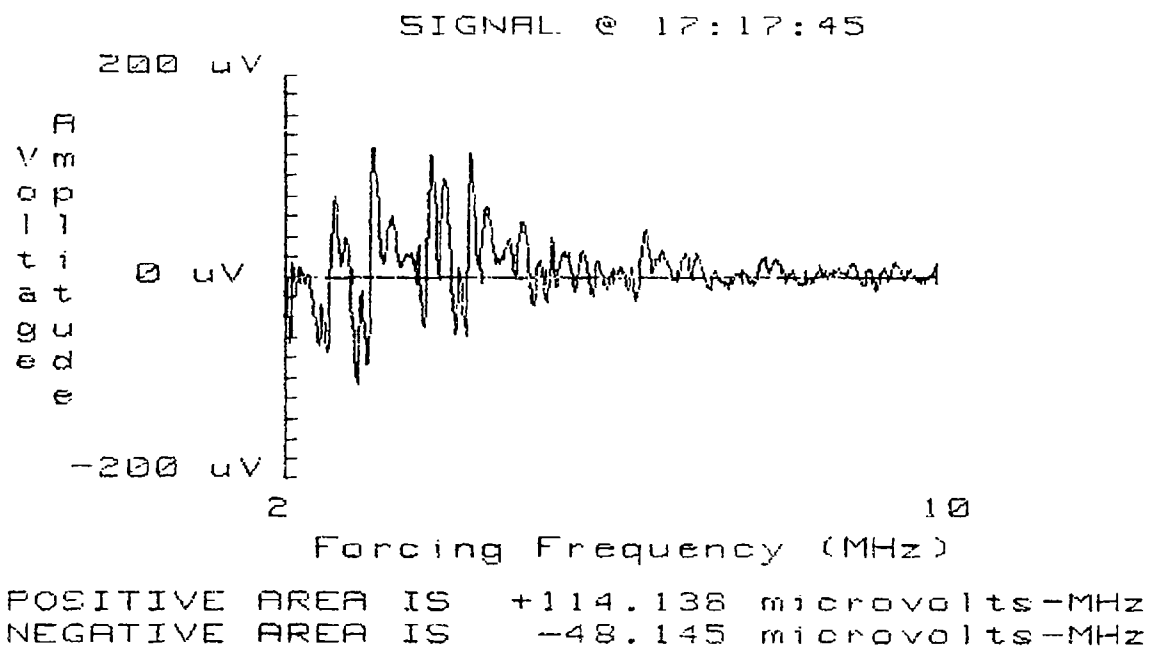
FIGURE 2B: OUTPUT SIGNAL; ACOUSTICAL TARGET IS A 3 MM-THICK PAAM GEL MOUNTED ON WALL-GONE; SIGNAL MINUS BACKGROUND.

19

PAAm gel simultaneously. Because the signal from the back surface has travelled $2 \cdot 3$ mm = 6 mm farther (or ~0.4 μsec longer), its offset frequency should be ~160 Hz higher. The range mode output does in fact show two distinct frequency components separated by 160 Hz. This is taken to mean that the signal analyzer is receiving two signals that differ in frequency by 160 Hz. When they are summed together for the FRC display, the beat phenomenon appears as a 160-Hz oscillation in the amplitude. Since the time of one measurement was 0.2 second, about 32 of these beats should appear in the FRC plot, as is the case.

IV. ATTEMPTS TO PREPARE SUITABLE CALIBRATION STANDARDS

For calibrating the bubble detector, it is necessary to have standards that are subject

to assay by some reliable independent method. We have prepared bubble samples of the

sort that we anticipate using as calibrants and used them in some preliminary

measurements intended to estimate the bubble detector's S/N ratio. We plan to use

calibrants consisting of bubbles trapped in transparent hydrogels and to assay them using

differential interference microscopy. Our approach is described below.

A. Methods

To produce the gels, aqueous solutions were prepared in the following compositions:

solution A
     0.20 g/cm^3 acrylamide monomer
     0.01 g/cm^3 N,N´-methylene-bis-acrylamide crosslinking monomer
     1.0 μl/cm^3 N,N,N´,N´-tetramethylethylenediamine accelerator

solution B
     variable 0.2-6 mg/cm^3 ammonium persulfate initiator

Prior to mixing the solutions, each was sparged with nitrogen to remove dissolved

oxygen, which inhibits many vinyl polymerizations[4]. Each solution was passed through a

filter having a 0.22-μm nominal pore size to remove particles that otherwise would

severely confuse the microscopic examination. Equal amounts of solutions 'A' and 'B'

then were mixed and the resulting solution was cast between either a pair of cleaned

glass plates or a glass microscope slide and a glass cover slip. In experiments during the

period covered by this report, the plates (or the microscope slide and cover slip) were

separated by a 150 μm-thick plastic spacer designed for use in casting electrophoresis

gels. The monomer solution 'sandwich' was placed under vacuum for a few minutes (variable length of time). The polymerization was then allowed to proceed at ambient pressure at least until gelation occurred. Bubbles that formed by cavitation at the reduced pressure were trapped in the finished gel.

In some experiments the monomer solution was chilled to 0 °C and maintained at that temperature before and during sparging with N_2, to increase the concentration of dissolved N_2. Thus, the overpressure in the monomer solution, defined as [partial pressure of dissolved gas] ÷ [hydrostatic pressure], would be higher under vacuum and would persist even after the sample had been returned to ambient hydrostatic pressure. In other experiments, a detergent (Tween 40) was added to the monomer solution to reduce the surface tension.

In order to be useful, the calibration standards must be the same size when they are interrogated ultrasonically as when they were assayed microscopically. Accordingly, the stability of these bubbles over time was tested by examining some of them under a bright field microscope over several hours' time while leaving the gel membrane sandwiched between the glass plates. Our plan was to assay the calibration standards microscopically and use the bubble detector to interrogate them within 24 h of their production; during that time their dehydration would be prevented by storage in an enclosed container whose interior was kept at the dew point by the presence of standing water.

B. Results

Briefly, *free* bubbles that initially were smaller than 50 μm in diameter survived no more than a few hours before disappearing in any of the experiments. Bubbles larger

than $100 \mu m$ survived for many hours, although their sizes were not measured accurately enough over time to allow a more precise statement about their size stability. Adding detergent to the monomer solution or keeping the monomer solution chilled during sparging with N_2 dramatically increased the number of bubbles formed, but neither treatment had the effect of stabilizing the small bubbles over several hours. Bubbles formed spontaneously at ambient pressure in the chilled monomer solution upon its removal from the ice bath.

The shrinkage and disappearance of bubbles was easily viewed at magnification $100\times$. The collapsing bubbles left behind spherical, water-filled cavities in the gel matrix that were clearly visible as discontinuities. By staining the gel with food coloring we could be sure of which spherical cavities contained gas and which contained water -- the gas phases transmitted more light since the dye was excluded from them.

In some experiments, a thin film of bone wax was smeared onto one spot on a microscope slide before the monomer solution was cast onto the slide. Bone wax is very hydrophobic and was found to be an excellent nucleation site, as expected. Even small bubbles persisted many hours on the bone wax. This was expected because the bone wax presents an irregular surface with numerous crevices, and it is known that some bubbles in crevices can remain static indefinitely[5]. However, they are unsuitable for use as calibration standards because no reasonably complete mathematical description of the nonlinear dynamics of either non-spherical bubbles or of bubbles at a solid boundary is available.

V. SIMULATION OF THE GROWTH AND SHRINKAGE OF BUBBLES IN A CLOSED SYSTEM WITH FINITE SURFACE TENSION

A requisite for calibration standards for the bubble detector is that the bubbles must remain constant in size for enough time to permit their examination under a microscope and their ultrasonic interrogation. This means that they must be stable over a period of at least a few hours.

To give us an idea of how such stable calibrants might be prepared, a model was developed that predicts bubble diameter changes as a function of time in a closed system. Ideally, one would do this by solving the unsteady state continuity equation with radial symmetry. However, the continuity equation for this system is partial differential equation (PDE) because of the spatial, as well as temporal, variation in solute concentration. Solving a PDE was felt to be more time-consuming than this analysis warranted. Instead, we simplified the mathematics considerably by assuming that the flux of gas from the bubble surface is proportional to the mass transfer coefficient evaluated for a sphere in a quiescent liquid at steady-state (see Equations [4] and [11] below). The assumption of steady-state implies that the radius of the sphere, the solute concentration at the surface of the sphere, and the solute concentration far from the sphere, all are time-invariant. We also neglected the convective flux associated with bulk flow toward or away from the sphere as its size changes. All of the above simplifications are justified when the bubble size is changing sufficient slowly, and therefore are suitable for a study whose goal was to identify conditions leading to time-invariant bubble sizes.

24

Thermal, viscous, and compressibility effects were ignored, which invalidates the model at very small diameters (i.e., below 10 μm for a surface tension of 73 dyn/cm), when implosion is rapid and internal pressures are high. This is inconsequential for our application: first, we are uninterested in knowing precisely when a fast-shrinking bubble disappears; second, the system *in toto* is unaffected by these very small bubbles because they contain too little gas to be of consequence. The partial pressure of water in the gas phase is taken to be the vapor pressure of water at ambient temperature. Its dependency on either hydrostatic pressure and temperature is ignored, but again, these effects are significant only for tiny bubbles.

A. Mathematical details

For a single spherical bubble the mole flux of gas away from its surface is

$$J = k (C^{surf} - C^{\infty}) \qquad [4]$$

where J = mole flux, mol/(cm^2-sec);

    k = external mass transfer coefficient, cm/sec;

    C^{surf} = concentration of dissolved gas at the outer bubble surface, mol/cm^3;

    C^{∞} = concentration of dissolved gas far from the surface, mol/cm^3.

We now make the following reasonable assumptions:

a. There is equilibrium between phases across the phase interface.

b. There is no resistance to mass transport in the gas phase, so that the partial pressure of gas at the inner bubble surface "P^{surf}" simply equals its bulk value "P^{bub}" in the bubble.

c. The concentration of dissolved gas C_{dis} is related to the partial pressure of gas with

25

which it would be in equilibrium P_{dis} according to a concentration-independent partition coefficient K (i.e., $C_{dis} = KP_{dis}$), which is a statement of Henry's Law.

Equation [4] now becomes

$$J = k K (P^{bub} - P^{\infty}) \qquad [5]$$

We further note that P^{bub} equals the difference between the hydrostatic pressure within the bubble and the vapor pressure of H_2O, and we account for the surface tension effect:

$$P^{bub} = \wp + 2\sigma/R - P_{H2O} \qquad [6]$$

where $\wp$ = ambient hydrostatic pressure, dyn/cm^2;

σ = surface tension, dyn/cm.

The mass balance on the gas inside the bubble (assuming sphericity) gives us

$$J = -1/(4\pi R^2) \, dn/dt \qquad [7]$$

where R = bubble radius, cm;

n = number of moles of gas inside the bubble, mol.

Assuming ideal gas, we have

$$n = [P^{bub}(4/3)\pi R^3]/(R_G T)$$

$$= [(\wp + 2\sigma/R - P_{H2O}) (4/3)\pi R^3]/(R_G T) \qquad [8]$$

26

and
$$dn/dt = 4\pi/(R_G T) [(\wp - P_{H2O})R^2 + (4/3)R\sigma] dR/dt \qquad [9]$$

where R_G = gas law constant, 82.057 atm-cm^3/mol-°K;

. T = absolute temperature, °K.

We can now combine Equations [5], [6], [7], and [9] to yield an ordinary differential

equation for the rate of change of the bubble radius:

$$dR/dt = \frac{- kKR_G T (\wp - P_{H2O} + 2\sigma/R - P^\infty)}{[\wp - P_{H2O} + (4/3)\sigma/R]} \qquad [10]$$

To compute the mass transfer coefficient we use the result that, for a sphere in a

quiescent liquid at steady-state the dimensionless Sherwood Number is 2.0[6], so that

$$Sh = 2.0 = 2Rk/D$$

or $\quad k = D/R \qquad [11]$

where D is the diffusivity (cm^2/sec). Substitution into Equation [10] gives

$$dR/dt = \frac{- DKR_G T (\wp - P_{H2O} + 2\sigma/R - P^\infty)}{R [\wp - P_{H2O} + (4/3)\sigma/R]} \qquad [12]$$

Or, when more than one bubble is present, we can write Equation [12] in this form for

bubble i:

27

$$dR_i/dt = \frac{- DKR_GT (\wp - P_{H2O} + 2\sigma/R_i - P^\infty)}{R_i [\wp - P_{H2O} + (4/3)\sigma/R_i]} \qquad [13]$$

Equation [12] or [13] is easily solved analytically for the special case of constant P^∞, that is, an infinitely large system in which the bubbles have no effect on the bulk concentration of dissolved gas. For the *finite* closed system, a mass balance shows that

$$dC^\infty/dt = K\, dP^\infty/dt = -(1/V_L) \Sigma \, dn_i/dt \qquad [14]$$

for $i = 1$ to N bubbles, where V_L = the volume of the condensed phase, in cm^3. Then for each bubble i, Equation [9] can be substituted into Equation [14] to yield

$$-K\, dP^\infty/dt = 4\pi/(V_LR_GT) \Sigma ([(\wp-P_{H2O})R_i^2 + 4/3R_i\sigma] \, dR_i/dt) \qquad [15]$$

This is integrated to yield

$$P^\infty = P_0^\infty - 4\pi/(3KV_LR_GT) [(\wp-P_{H2O})(\Sigma R_i^3 - \Sigma R_{0,i}^3) + 2\sigma(\Sigma R_i^2 - \Sigma R_{0,i}^2)] \qquad [16]$$

where P_0^∞ = initial partial pressure of dissolved gas in the condensed phase, atm. All summations are from $i = 1$ to N, where N is the number of bubbles.

Therefore, Equations [13] and [16] define this system; Equation [13] must be solved for each bubble in turn, simultaneously with Equation [16]. We did this using a 4th-order Runge-Kutta numerical routine.

B. Simulation results

Understanding the simulation results is easier if one keeps in mind the definition of 'critical radius'. This is the radius of a bubble that would be in both mechanical and thermodynamic equilibrium with the condensed phase, so that there would be no mass flux at its surface and its size would not change with time. To derive an expression for R_{crit}, remember that the driving force for mass transport is $(P^{bub} - P^{\infty})$, or

$$\text{driving force} = (P + 2\sigma/R - P_{H2O} - P^{\infty}) \qquad [17]$$

A quasi-stable bubble thus can be defined mathematically as one for which the right side of Equation [17] is near zero; that is, $P^{bub} = P^{\infty}$. R equals the critical radius when the driving force *is* zero, so we can solve Equation [12] for the critical radius:

$$R_{crit} = 2\sigma/(P^{\infty} + P_{H2O} - P) \qquad [18]$$

When $R > R_{crit}$ the bubble grows and when $R < R_{crit}$ it shrinks. In an unbounded system where P^{∞} = constant the growth or shrinkage is monotonic. In a finite system in which P^{∞} is a time-dependent variable, a bubble may alternately grow and shrink as P^{∞} fluctuates and R_{crit} fluctuates with it.

29

To further understand the simulation results, it should be noted that two bubbles of different sizes cannot simultaneously be equilibrated with the same condensed phase because their internal pressures differ, and that a larger bubble must always be either growing faster or shrinking slower than a smaller bubble. These observations lead to the conclusion that any closed system must ultimately reach one of two possible final states:

1) all of the bubbles have collapsed, or

2) only one bubble remains, and it is the one that was largest initially.

So, we see that bubbles initially grow or shrink depending upon whether their radii are greater than or less than the initial critical radius of the system. Each bubble later grows or shrinks depending upon the current value of R_{crit}, which depends on the history of bubble size changes in the system. Ultimately, all of the bubbles collapse or else only one bubble remains.

Unless specially noted, the example simulations to be discussed were computed at the following conditions:

ambient pressure P = 1 ATA;

temperature T = 293.16 °K (20 °C);

surface tension σ = 72.75 dyn/cm (its value at 20 °C for the air/H_2O system);

vapor pressure of water P_{H2O} = 0.02307 atm (its value at 20 °C);

volume of the condensed phase V_L = 0.015 cm^3;

diffusivity = $3 \cdot 10^{-5}$ cm/sec, which is its approximate value for nitrogen in H_2O
    at 20°C[7];

partition coefficient K = $6.34 \cdot 10^{-7}$ mol/(cm^3-atm), which is its approximate value
    for nitrogen in H_2O at 20 °C[8].

The system volume V_L also will be seen to be critical to this analysis. Its value of 0.015 cm^3 was chosen because this is the volume of a membrane of dimensions 1 cm × 1 cm × 150 μm, which are roughly the expected dimensions of a calibration standard.

Figure 3 shows simulation results for a case in which five relatively small bubbles are posited in a condensed phase originally containing a partial pressure of 1 atmosphere absolute (1 ATA) of dissolved gas. R_{crit} in this system initially is 60 μm (the critical diameter is 120 μm). All of the bubbles eventually collapse, the smaller ones disappearing first; the partial pressure of dissolved gas eventually rises to 1.004 ATA but this is not high enough to prevent the largest bubble from collapsing, i.e., to bring $R_{crit} < R$ for the largest bubble.

In the second example, shown in Figure 4, all conditions are the same as in Figure 3 except for the initial sizes of the bubbles. Two of the bubbles initially are larger than the critical diameter of 120 μm. An inspection of the numerical results from which this plot was made shows that the bubble that initially is 180 μm in diameter grows slowly for 23 h and then begins to shrink very slowly as P^∞ is depleted by the largest bubble, which will continue its slow monotonic growth as it asymptotically approaches equilibrium with the rest of the closed system.

A pseudo-stable state is reached in Figure 4 because two of the bubbles are large enough to significantly influence the amount of dissolved gas. Growth of a sufficiently large bubble always reduces the driving force for diffusion to that bubble by depleting P^∞, and shrinkage of a sufficiently large bubble always reduces the driving force for that

Figure 3: Bubble size changes; "Small" bubbles, initial partial pressure of dissolved gas = 1 ATA

32
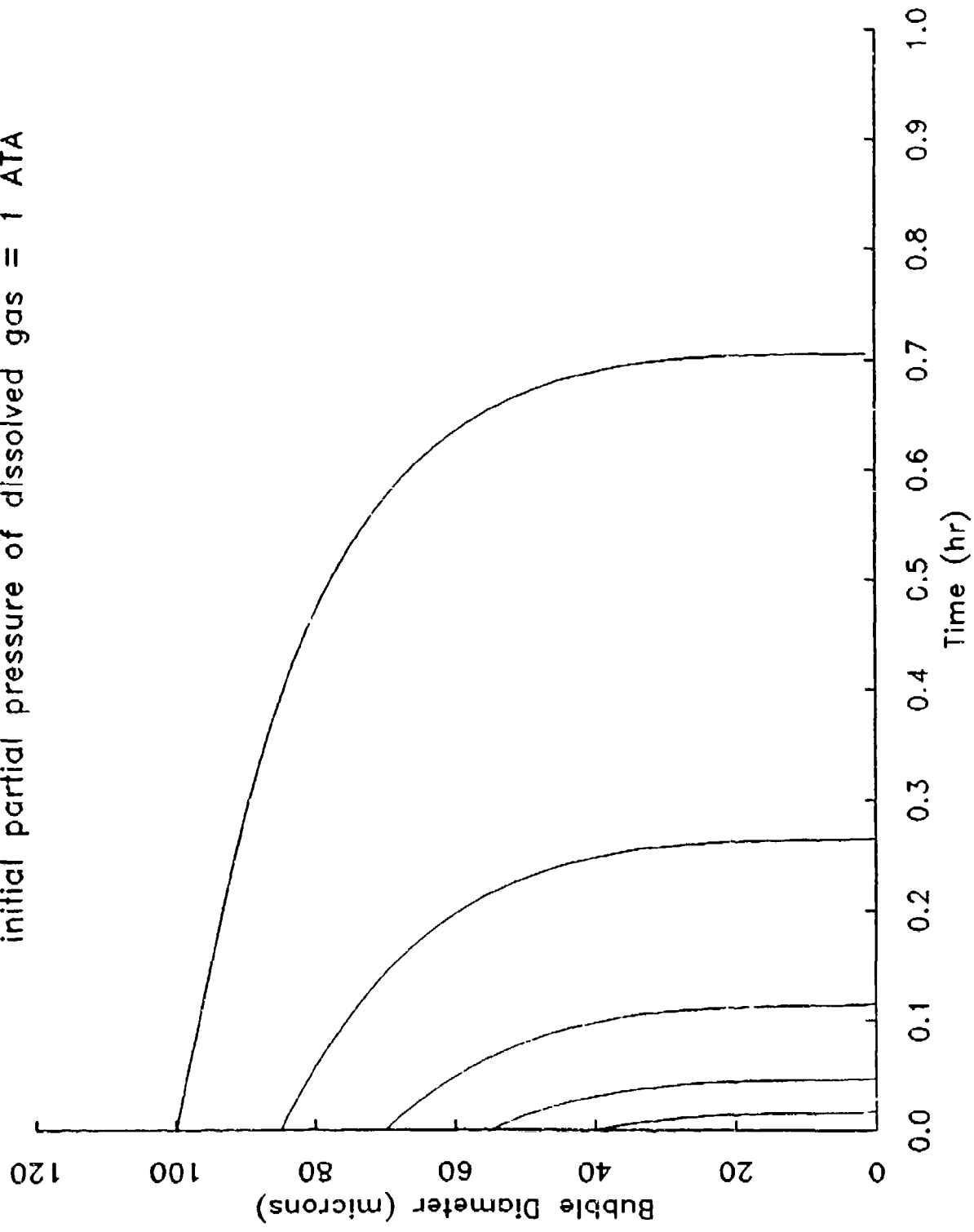
Figure 4: Bubble size changes; Some "large" bubbles, initial partial pressure of dissolved gas = 1 ATA

33
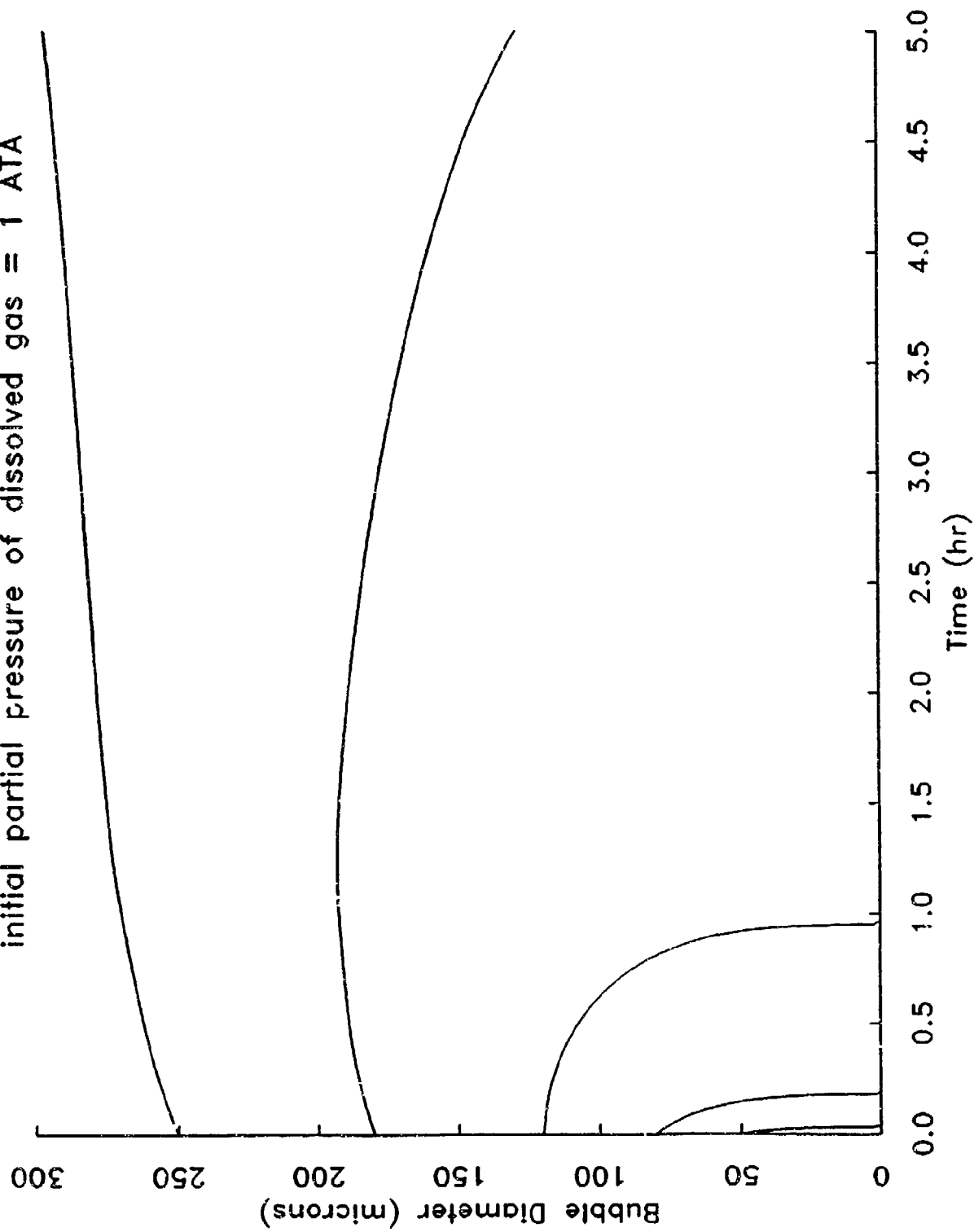
bubble by augmenting P^∞. Sufficiently small bubbles won't affect P^∞ enough to stabilize their sizes.

In Figure 5, we see an instance of a substantial initial overpressure in the condensed phase. The initial P^∞ is 3 ATA, giving a critical diameter of 1.4 μm. Although it is difficult to see on the plot, the bubbles initially are very different in size, ranging from 5 μm to 200 μm diameter. They all grow rapidly at first; the smaller ones begin shrinking as P^∞ declines. At time = 5.8 h, P^∞ has been reduced to 1 ATA by the bubble growth. Eventually, only one bubble will remain. But, after about 6 h the bubbles are almost static in size over many hours. This is because the driving force for mass diffusion is small since $P\sim P^\infty$ and the surface tension term $2\sigma/R$ is small (see Equation [15]).

It is evident from studying Figures 4 and 5 that bubbles having diameters much greater than 100 μm remain fairly static in size over several hours when the overpressure is small and the surface tension is that of the air/H_2O system. That is, they are pseudo-stable for our purposes. Bubbles much smaller than 100 μm cannot be stabilized at a surface tension of 73 dyn/cm.

Figure 6 illustrates a simulation done with the surface tension set at σ = 5 dyn/cm, which may be possible to achieve using surfactants. The initial value of P^∞ is 1 ATA, so that a slight 'overpressure' exists only because of the contribution of water vapor. Still, the critical diameter is only 8.6 μm because of the low surface tension. None of the bubbles is larger than 60 μm diameter at the start. The results are qualitatively similar to those in Figure 5 in that we eventually obtain a pseudo-stable system after an initial

34

Figure 5: Bubble size changes;
initial partial pressure of dissolved gas = 3 ATA

35

Figure 6: Bubble size changes; "Small" bubbles, initial partial pressure of dissolved gas = 1 ATA, surface tension = 5 dyn/cm
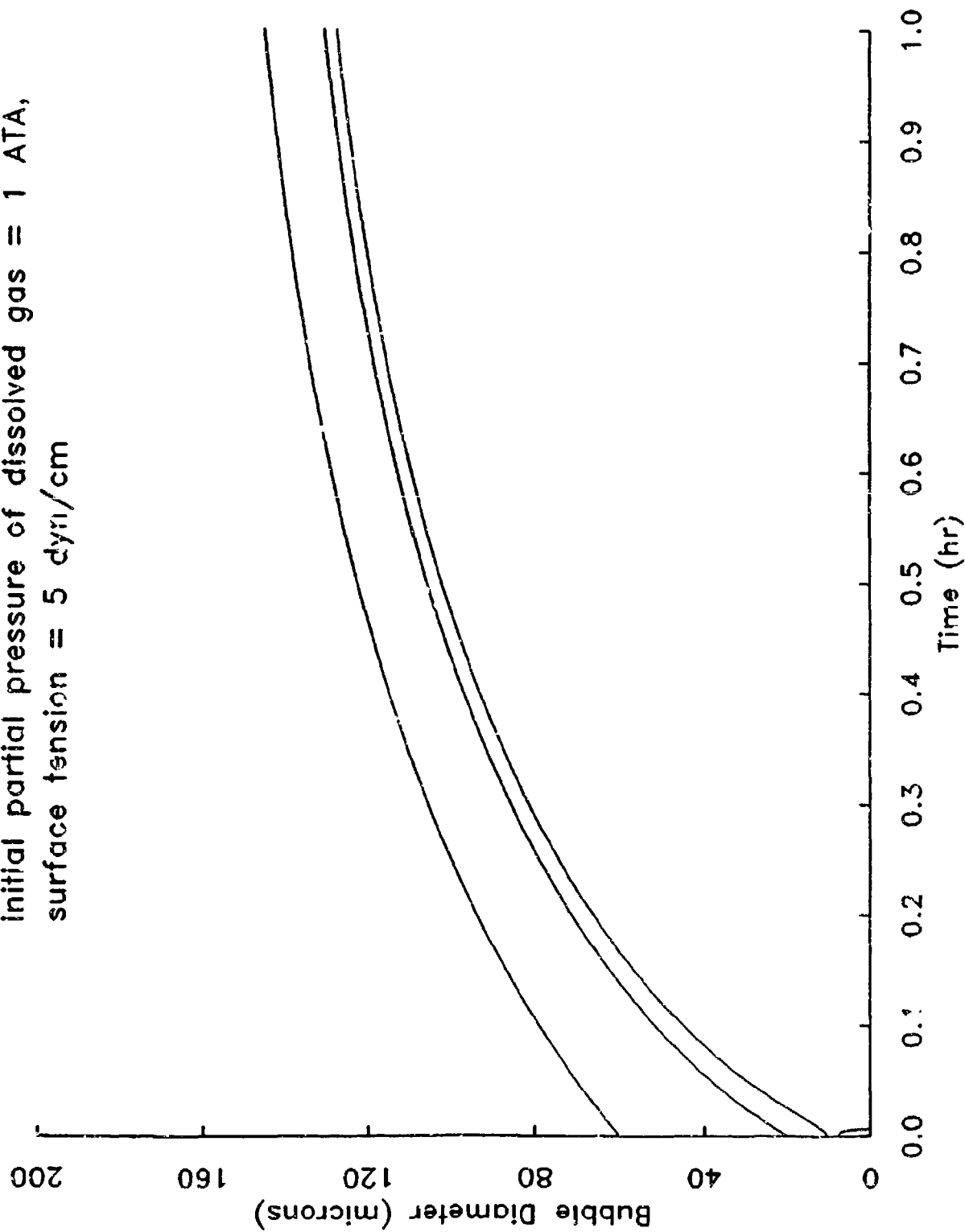
period of relatively rapid changes. The stability again occurs because of the small driving force, with $P-P^\infty$ and $2\sigma/R$ being small. In this hypothetical system we have succeeded in stabilizing bubbles smaller than 200 μm.

Can bubbles smaller than 20 μm be stabilized if both the surface tension and the overpressure are *extremely* small? In Figure 7, P^∞ is 0.99 ATA initially, the surface tension is 5 dyn/cm, so the critical diameter is 15 μm. The bubbles are initially 5, 10, 15, 20, and 30 μm in diameter. The bubbles that begin life with diameters of 15 μm or less still are not stabilized: they all collapse within 36 h. The larger bubbles, which grow, will not stabilize until they are large enough to deplete the dissolved gas surrounding them; this does not happen within the first 100 h of the simulation, by which time they both are larger than 90 μm in diameter. It does not seem possible to maintain stable bubbles smaller than ~100 μm without an implausibly large concentration of bubbles, although it certainly would be possible in a much smaller system.
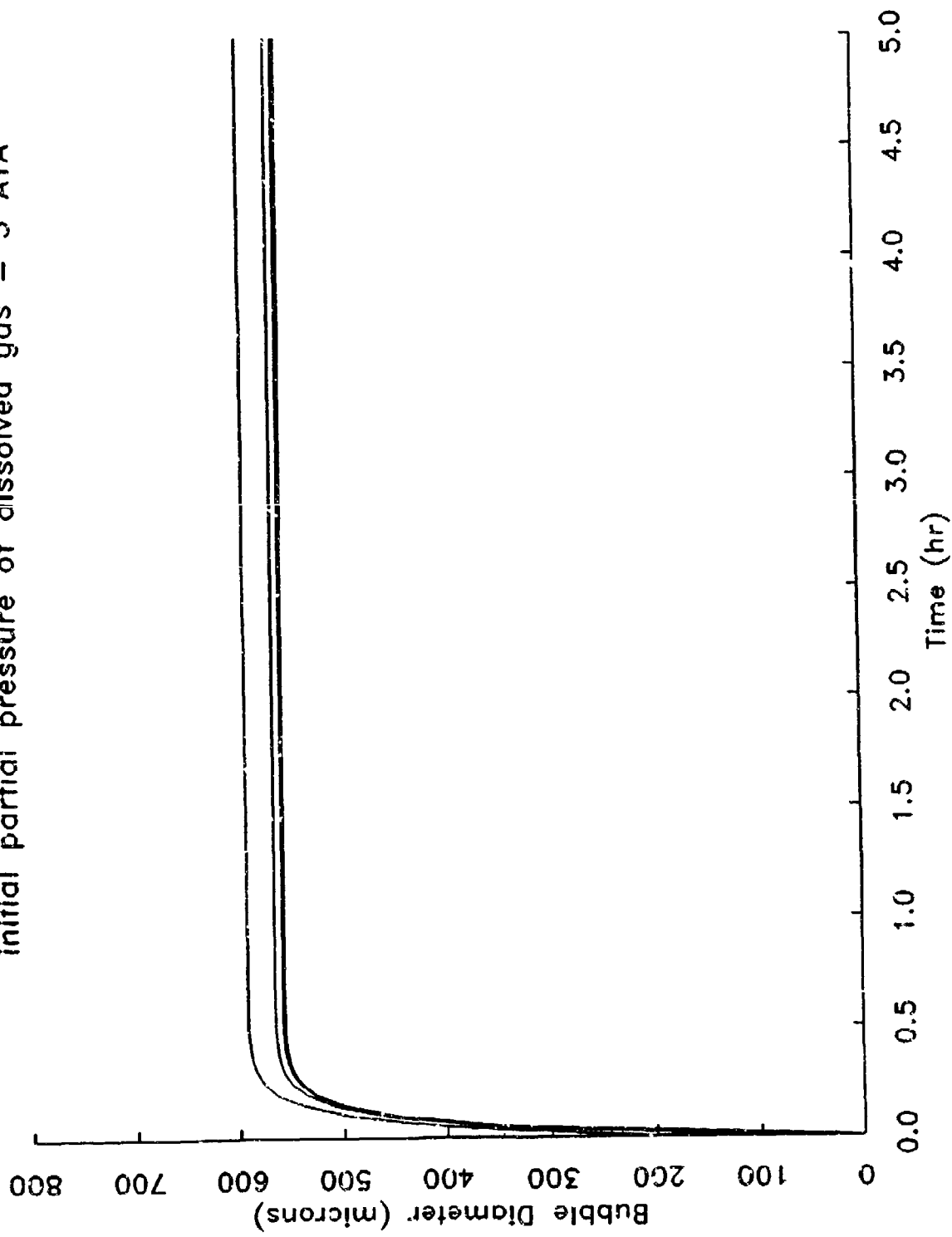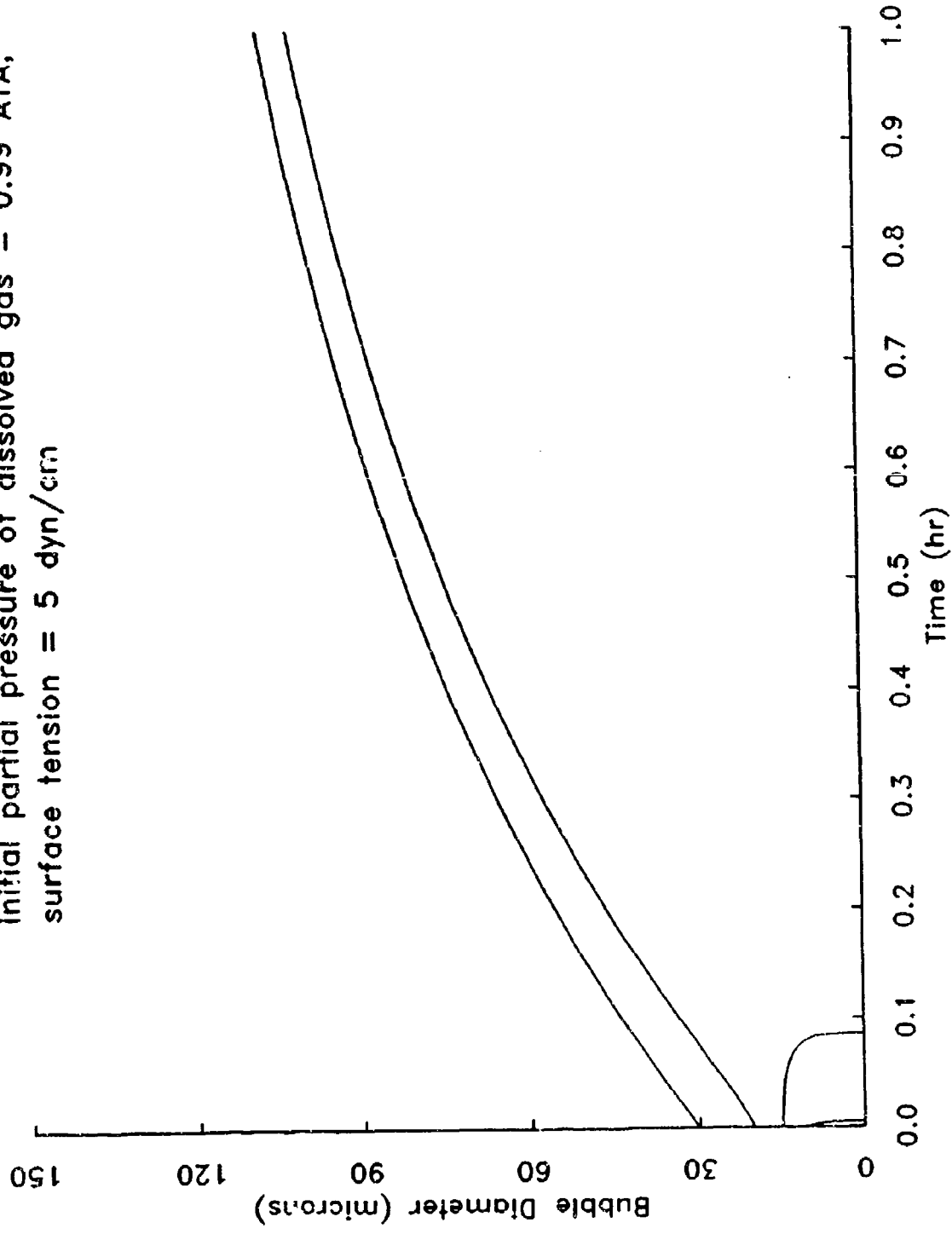
Figure 7: Bubble size changes; "Small" bubbles, initial partial pressure of dissolved gas = 0.99 ATA, surface tension = 5 dyn/cm

38

VI. NOISE MEASUREMENTS

We attempted to quantify the amount of electronic noise generated by the system's various noise sources. Of primary interest is the amount of noise present when the divide-by-2 circuit is in use, because this is the output from which we hope to deduce bubble sizes by analyzing the 2nd harmonic component of the sound radiated from bubbles. Because the amplitude of harmonic distortion products normally depends on the amplitude of the input signal, the 2nd harmonic noise should increase with the amplitude of the input signal. This is borne out by the data.

A. Approach and methods

In the following discussion, we report the ratio, in decibels (dB), of V^{2h} to V_{max}^{fund} for various input voltage levels, where V^{2h} is the RMS (root mean square) voltage amplitude of the 2nd harmonic distortion and V_{max}^{fund} is the maximum possible RMS amplitude voltage of the fundamental component of the output signal. V_{max}^{fund} was measured by reflecting the transmitted signal off of the surface of a lead brick with the divide-by-2 circuit bypassed; lead is an excellent sonic reflector because of the mismatch in mechanical impedance between lead and water, and the observed output signal amplitude therefore is taken to be maximized in this experiment for a given input voltage amplitude.

V^{2h} was measured by reflecting the transmitted signal off of a slab of Wall-Gone rubber sound absorber with the divide-by-2 circuit in use and no bubbles apparent. Using Wall-Gone as the acoustical target is more realistic as a physiological analogue

39

than measuring noise with a hard target in place. Although ideally we might expect the signal in this configuration to be immeasurably small, in fact we observe a substantial 2nd harmonic component generated by 2nd harmonic distortion in the front end components (consisting of the transducers, the divide-by-2 circuit, a power amplifier in line between the signal generator and the transmitting transducer, and a mixer), and by nonlinear vibration of the Wall-Gone rubber. On the other hand, noise levels are considerably lower with Wall-Gone as the target than with a hard target, because less energy is reflected to the receiving transducer from the Wall-Gone than from a hard target.

The scheme for characterizing noise levels using the ratio V^{2h}/V_{max}^{fund} was chosen because the results are relevant to the system's S/N ratio for measurements of gas bubbles. Although the reader probably finds this elevance mysterious now, we will explain it in section VIII, 'Estimating the Signal/Noise Ratio'. Note for now that V^{2h}, not V_{max}^{fund}, is considered the magnitude of noise.

All mea ements were made under the following conditions:

"range" mode in use
sweep time = 0.1 sec
span = 4 kHz (therefore, time record length = 0.1 sec)
sweep start frequency = 0.2 MHz
sweep st frequ = 5 MHz
windowing = flattop
signal averaging: 20 time records averaged
target distance ~ 3.25 cm

Recall from the Introduction that, in the range mode, the output signal appears as a spectrum of voltage amplitude versus offset frequency Δf, where Δf is proportional to the distance from the transducer head to the target. In the experiments of this section the output spectrum contained a voltage spike at a frequency $\Delta f \sim 2.1$ kHz, which corresponds to a distance of 3.25 cm in water. The reported voltage was read at the maximum of the peak at 2.1 kHz. Noise at other frequencies was negligible compared with the noise at 2.1 kHz.

B. Results

Table 1 shows the noise level measured over a five-fold range of input voltage levels. Inspection of the rightmost column in the table reveals that the noise level is essentially constant at ~-37 dB relative to the maximum output signal level at input voltages greater than 2 V.

As an incidental (but important) observation, we see from the entries in the third column that the system's frequency response (i.e., output voltage at the fundamental frequency $\div$ input voltage) is nearly linear over the input voltage range of 2.5 to 4 V peak-to-peak from the signal generator, suggesting that this is an advantageous operating range. From additional measurements (not shown) it has been observed that the linear frequency response occurs over the same range of input amplitudes even when Wall-Gone is the acoustical target. The substitution of Wall-Gone for lead attenuates the output signal by 94% consistently, regardless of input amplitude. It is suggested therefore that the appearance of nonlinear frequency response is a much stronger function of V_{in} than of V_{out}.

41

TABLE 1: System Noise

voltage setting on 3325A signal generator	V^{2h}	V_{max}^{fund}	V^{2h}/V_{max}^{fund}
1 V peak-to-peak	47.42 μV RMS	0.793 mV RMS	- 31 dB
1.5	90.78	1.523	- 35
2	136.1	2.288	- 36
2.5	181.0	3.032	- 36
3	229.6	3.826	- 37
3.5	268.7	4.431	- 38
4	301.6	4.969	- 37
4.5	332.1	5.398	- 37
5	357.3	5.781	- 37

VII. THEORY OF VIBRATING BUBBLES

A. Approximate analytic solutions via the perturbation method

The motion of a free, spherical gas bubble in an incompressible condensed phase has been described by solving the equation of motion, i.e., the momentum balance, for the condensed phase. This equation is found to be an ordinary nonlinear differential equation. Since the system is spherically symmetric (given a homogeneous, isotropic medium) the only spatial dimension of importance is the radial coordinate r. If the equation is written at the outer bubble surface, we obtain[9,10]

$$RR'' + (3/2)(R')^2 = 1/\rho_L[P_{in}(t) - 2\sigma/R - \tau_R] \qquad [19]$$

where $R = R(t)$ is the bubble radius at time t, cm;

$R' = dR/dt$;
$R'' = d^2R/dt^2$;
ρ_L = density, g/cm^3;
$P_{in}(t)$ = the pressure at the inner surface of the bubble at time t, atm;
σ = surface tension, dyn/cm;
τ_R = radial stress at the outer bubble surface, dyn/cm^2.

The term τ_R arises when we apply the boundary condition that radial stresses are continuous across the bubble surface. In section C we show how this stress term is rewritten in terms of strain or rate of strain, depending on what constitutive equation is valid for the condensed phase. For now, let us assume that the bubble resides in a

43

Newtonian fluid. In section C we will show that this leads us to calculate $\tau_R = \wp^{out} + 4\mu R'/R$, where $\wp^{out}$ is the hydrostatic pressure at the outer surface of the bubble.

Prosperetti[10,11] found an approximate, analytic solution to Equation [19] for a sinusoidally oscillating ambient pressure, that is for a bubble in an externally applied sound field. The mathematics are quite complicated and we will only summarize some of the major features here. For more details see the Appendix of reference 1. For a reasonably complete discussion of the mathematics one must look to Prosperetti's papers[10,11].

Prosperetti replaces $\wp^{out}(t)$ with $\wp_0(1-\epsilon\cos(\Omega t))$, i.e. $\wp_0$ is the mean ambient pressure, ϵ is the amplitude of sound waves imposed on the bubble, and the frequency of that sound is Ω. The internal pressure $P_{in}(t)$ is represented by a polytropic expression $P_{in} = P_{in,eq} (R_0/R(t))^\kappa - 4\mu_{th}R'/R_0$, where R_0 is the equilibrium radius, κ is the "effective polytropic exponent", $P_{in,eq}$ is the internal pressure corresponding to $R=R_0$, and μ_{th} is a so-called 'thermal viscosity' introduced as an *ad hoc* corrective term to compensate for the polytropic expression's inability to account for phase shifts between pressure and temperature. Prosperetti also defines an 'acoustic viscosity' μ_{ac} that arises from momentum transfer from the bubble to the liquid. The thermal and acoustic viscosities have the same units as a "real" viscosity and each is a "damping" term, meaning that it appears in the momentum balance as a multiplier to the velocity term R'. Accordingly, Prosperetti combines all three viscosities into an "effective viscosity" $\mu_{eff} = + \mu_{th} + \mu_{ac}$. Equation [19] now becomes

$$RR'' + (3/2)(R')^2 =$$

$$1/\rho_L[\ P_{in,eq}\ (R_0/R(t))^{3\kappa} - \wp_0(1-\varepsilon\cos(\Omega t)) - 2\sigma/R - 4\mu_{eff}R'/R\ ] \qquad [20]$$

Expressions for the polytropic exponent, thermal viscosity, and acoustic viscosity all are calculated from a separate analytic solution to the system of six partial differential equations that comprise the <u>linearized</u> equations of continuity, motion, and energy in both phases. The condensed phase is considered compressible in the linearized governing equations, even though the nonlinear Equations [19] and [20] are written for incompressible liquids. (In fact, the acoustic damping term is zero for an incompressible medium.) Linearized equations are valid for small perturbations from equilibrium -- in this case, for small amplitude vibrations -- but keep in mind that no information on harmonics, subharmonics, or phase shifts is contained in a linearized treatment of a vibrating system. The mechanics of solving this system of equations are exceptionally complicated.

Next, the substitution $R(t) = R_0 (1 + x(t))$ is made into equation [20]. The dimensionless variable 'x' is seen to be a fractional perturbation of the bubble radius $R(t)$ from its equilibrium value R_0. The problem is made tractable by discarding all x, x', and x'' terms that are raised to powers of 4 or greater, but note that retaining the 2nd and 3rd power terms retains the essential effect of the nonlinearity (provided x is small).

Finally, algebraic solutions to the resulting equation are obtained by a "perturbation" technique first advanced by Krylov, Bogolyubov, and Mitropolsky[12]. Each solution is valid when the forcing frequency Ω is 'near' one of the system's resonance frequencies.

45

We are particularly interested in the 2nd harmonic component of the solutions, which is found by retaining only the terms that are of frequency 2Ω, since that component will be measured by the bubble detector. It turns out that the mathematical system (and presumably the physical system likewise, if its mathematical description is accurate) is 'catastrophic': as the forcing frequency is swept through the various resonance frequencies there are discontinuous jumps between stable solutions, and there is hysteresis behavior that causes the location of these jumps to depend on whether the forcing frequency is being swept upward or downward.

The procedure summarized above yields an algebraic expression for the amplitude of the oscillations of R as a function of forcing frequency and all other relevant parameters. This is readily converted to the amplitude of the radiated pressure wave corresponding to it, denoted $\|P_{rad}\|$, by solving the linearized 'wave equation' in the liquid (in fluid mechanics a wave equation is simply the equation of motion written for a compressible medium in which a wave is being propagated). If desired, only the 2nd harmonic component of the radial oscillations can be included, and we designate the pressure amplitude of that component as $\|P_{rad}{}^{2h}\|$.

The fact that the values of the parameters 'κ' and 'μ' (used below) are estimated using first order expansions (linearizations) of the terms in the mass, energy, and momentum balances means that they are valid only for a linear system. Their usage when analyzing this nonlinear system is an *ad hoc* approach necessitated by the difficulty of the mathematics.

Clearly, the analytic solution incorporates several questionable assumptions and

46

computational simplifications. Its value is that it can be computed rapidly enough to make it useful in the iterative data-fitting routine mentioned in the Introduction to this report, with which the equilibrium bubble radius R_0 will be estimated for an unknown bubble by comparing observed resonance frequencies with the predicted values.

B. Numerical solutions via the Galerkin Spectral Method

Given our reservations about the reliability of the analytic solution discussed in section A, we would like to have a means of numerically solving the equations governing a vibrating bubble without resorting to so many simplifying assumptions. This new solution could be used to evaluate the accuracy of the analytic solution in the absence of direct experimental verification, which is unlikely to appear any time soon. We are willing to trade computational economy for accuracy with the numerical solution.

Kamath and Prosperetti[13] used a Galerkin spectral method to solve the governing equations and found significant deviations of the analytic solution from the numerical results when the driving amplitude was high enough. As will be discussed shortly, the mathematical description that Prosperetti evaluated using the Galerkin method is in some ways more sophisticated, in other ways more simplified than the description he evaluated earlier using a perturbation technique. This confuses a comparison of the results from the two solutions. The reader should look to reference 14 for an overview of Galerkin techniques. Here, we will review the particulars of how Prosperetti (and we) used the Galerkin spectral method on our system.

The Galerkin method is used to reduce the partial differential equations to a system of ordinary differential equations, which subsequently are solved using the Gear method.

47

The result consists of the value of R, the bubble radius, as a function of time at some forcing frequency Ω. This time domain information can be converted to an amplitude spectrum via Fourier transformation. To get the _steady state_ solution one integrates until steady state oscillations are attained, then Fourier transforms the time domain data from only the last oscillation cycle. If one is interested in the amplitude of only the 2nd harmonic component as a function of Ω, then the amplitude at frequency 2Ω is extracted from the spectrum. Once the steady state radial amplitude at frequency 2Ω has been computed over a range of Ω's, we can construct the spectrum of amplitude versus Ω. Also, the amplitude of R at frequency 2Ω can be converted to $\|P_{rad}^{2h}\|$ by solving the aforementioned linearized wave equation in the condensed phase. In sections D and E, we will present results in an alternative form that does not involve Fourier transformation: we show the maximum bubble radius attained during a steady state oscillation.

In Prosperetti, Crum, and Commander,[15] simplified governing equations are derived from the conservation equations for mass, momentum, and energy for both the gas in the bubble and the liquid outside the bubble, along with boundary conditions at the gas-liquid interface (i.e., the bubble wall). Based on several reasonable assumptions, and several order of magnitude comparisons that show certain quantities to be negligible, the authors are able to reduce the original system of six partial differential equations (i.e., the conservation equations) to one partial differential equation and two ordinary differential equations.

Two basic assumptions are that the gas is perfect and the bubble maintains a

spherical shape. An order of magnitude argument shows that, near the main resonance frequency of a bubble in forced oscillation, the Mach number M_B of the bubble wall, referred to the speed of sound in the gas, is extremely small; i.e. $M_B = \dot{R}/c_G$ is close to zero. Using this approximation it can be shown[13] that the radial gradient in pressure inside the bubble is negligible compared with the temporal variation of pressure; i.e., the pressure is almost uniform spatially within the bubble. An estimate of viscous shear in the gas shows it to be negligible. Based on these results it can be shown that the momentum balance equation for the gas reduces to the simple statement that gas pressure is a function only of time.

Some further assumptions, which involve the bubble wall temperature and vapor effects, are less important, because the system equations would still be tractable without them. An order of magnitude estimate shows that, owing to the greater thermal inertia of liquid than gas, the temperature at the bubble surface is almost unperturbed from the ambient temperature provided there is not too much heat being alternately consumed and released by the evaporation and condensation of vapor. The authors ensure the validity of this approximation in their mathematical construct by neglecting vapor altogether. In the physical world, they suggest (based on their order of magnitude estimates) that the approximation is valid for bubbles in H_2O at temperatures up to about 50 °C. In other words, the liquid must be sufficiently cool. With the use of this approximation the equation of energy in the liquid phase can be dispensed with; otherwise, it would be needed for determining the boundary condition on the energy equation in the gas phase.

In addition, both slow and fast diffusion of the gas in and out of the bubble are known to have negligible dynamical effects. Thus, diffusion is ignored entirely and we assume the bubble boundary is impervious to the gas. Fast diffusion refers to diffusion with time scale the order of one period of the oscillation; slow diffusion (often called rectified diffusion) refers to diffusion with a time scale of, for example, thousands of periods in which the total gas contents and/or the equilibrium radius of the bubble may change.

Under the stated assumptions, the system of equations to be solved becomes:

a) Radial dynamics equation:

We use Keller's equation for a gas bubble in a compressible liquid.

$$(1 - \dot{R}/c)R\ddot{R} + 3/2(1 - \dot{R}/(3c))\dot{R}^2 \;=\;$$

$$1/\rho_L(1 + \dot{R}/c + (R/c)\,d/dt)p_B - 1/\rho_L(1 + \dot{R}/c)\,p_A(t + R/c) \qquad [21]$$

where $R = R(t)$ is the bubble radius at time t, ρ_L is the density of the liquid, 'c' is the speed of sound in the liquid, p_B is the pressure in the liquid just outside the bubble, and $p_A(t)$ is the ambient pressure (in radial equation P_A is evaluated at time = t + R/c). Keller's equation is valid when the Mach number of the bubble wall is sufficiently small so that quantities proportional to its square may be neglected. We assume $p_A(t) = p_\infty (1 - \epsilon \cdot \sin(\omega t))$. A balance of the normal stresses across the bubble surface yields:

50

$$p_B = p_B(t) = p - 2\sigma/R - 4\mu_L(\dot{R}/R)$$ [22]

where μ_L = liquid viscosity.

b) Pressure equation:

This equation relates the internal pressure to the temperature gradient. Since the internal pressure p is assumed to be uniform throughout the bubble; p is independent of r; it depends only on 't'.

$$\dot{p} = 3/R(\ (\gamma - 1)K\cdot(\partial T/\partial r)|_R\ -\ \gamma p \dot{R}\ )$$ [23]

c) Temperature equation:

This is also called the energy equation.

$$\gamma p/((\gamma - 1)T)\ [\partial T/\partial t\ +\ 1/(\gamma p)((\gamma - 1)K\ \partial T/\partial r\ -\ 1/3\ r\dot{p})\ \partial T/\partial r]\ -\ \dot{p}\ =\ \nabla\cdot(K\ \nabla T)$$ [24]

where K(T) is the thermal conductivity of air. Based on data for

$200\ °K < T < 3000\ °K$, Kamath and Prosperetti suggest using the linear function

$K(T) = 5.528\ T + 1165$.

Boundary conditions for system:

The temperature on the bubble surface equals the constant exterior temperature T_∞.

51

Initial conditions for system:

Bubble is at rest with equilibrium radius R_0.

Internal pressure has value $p_0 = (2 \sigma / R_0) + p_\infty$

Temperature is constant throughout bubble; its value is T_∞.

Let us define a scaled radial variable $y = r/R(t)$ to be used instead of r.

A dependent variable $\tau(y,t)$ is defined by $\tau = \int_{T_\infty}^{T} K(\theta) \, d\theta$ where K(T) is defined

above.

The Galerkin method is used to replace spatial partial derivatives (i.e., those involving the variable 'y') with finite linear combinations of Chebyshev polynomials $T_k(y)$. Specifically, we represent $\tau(y,t)$ as an infinite sum of shifted Chebyshev polynomials $\Phi_k(y) = T_{2k}(y) - 1$. Let the coefficients be denoted $a_k(t)$. Denote by τ_N the series truncated after N terms; $\tau_N = \sum_{k=1}^{N} a_k(t) \, \Phi_k(y)$

The pressure and temperature equations involve spatial derivatives. Using the expression for τ_N we can convert these spatial derivatives into finite linear combinations $\sum_{k=1}^{N} e_k(t) \, T_k(y)$ where the $e_k(t)$ are functions of the $a_k(t)$.

With these techniques, the temperature equation is reduced to a system of ordinary differential equations which can be integrated in time. Following Kamath and Prosperetti's approach we used a four-term Chebyshev expansion. The system must be integrated for many (usually more than 10) cycles before the system reaches steady-state oscillations. For certain parameter values there may be more than one stable solution; if

52

so, the solution that arises in any given problem will depend on the initial conditions used for that problem. In other words, the bistability/hysteresis effect, well established for the analytic solution with resonance frequencies (see the preceding section), appears as well in the numerical solution.

C. Derivation of the normal stress at the surface of a spherical cavity

The boundary condition on the equation of motion in the medium surrounding a bubble (Equation [19]) is different for a liquid than for a solid because different constitutive equations govern the mechanical behavior of the two types of media.

The continuity equation for an incompressible substance with spherical symmetry can be written either

$$(1/r^2) \, \partial(r^2 v_r)/\partial r = 0 \qquad\qquad [25a]$$
$$\text{or} \qquad (1/r^2) \, \partial(r^2 u_r)/\partial r = 0 \qquad\qquad [25b]$$

where v_r = radial velocity and u_r = radial displacement. Velocity is simply the time derivative of displacement: $v_r = \partial u_r/\partial t$. Integration yields

$$v_r = A_1(t)/r \qquad\qquad [26a]$$
$$\text{or} \qquad u_r = A_2(t)/r \qquad\qquad [26b]$$

where $A_1(t)$ and $A_2(t)$ are integration factors to be evaluated later. The boundary condition on the continuity equation is continuity of either velocity or displacement at

the bubble surface:

$$v_r|_{r=R} = dR/dt = R'$$ [27a]

or $$u_r|_{r=R} = R - R_E$$ [27b]

where R_E = bubble radius at which the medium surrounding the bubble is undeformed, which in general is _not_ the same as the equilibrium radius R_0. It follows from Equations [26] and [27] that

$$v_r = R^2 R'/r^2$$ [28a]

or $$u_r = R^2(R-R_E)/r^2$$ [28b]

The boundary condition on the equation of motion is continuity of the radial stresses across the phase interface[*]:

$$-P_{in} + 2\sigma/R = \tau_R$$ [29]

where τ_R is the radial stress at $r = R$.

---

[*] We are obeying the following incomprehensible arbitrary convention on signs of stress components, taken almost verbatim from reference 9:

The stress τ_{ij}, due to action _by_ material on the positive side of the surface _on_ the material on the negative side, is positive if the line of action is along positive spatial coordinate x_j.

Conversely, the stress exerted from the negative side of the surface on the material on the positive side is positive if the line of action is along negative x_j.

Now we will apply the constitutive equations. For a Newtonian liquid, the stress tensor components are linearly related to the components of the rate of strain tensor:

$$\tau_{ij} = -P\delta_{ij} + \Delta_{ij} \tag{30}$$

where P = hydrostatic pressure, atm;
  δ_{ij} = Kronecker delta, defined thus:
    δ_{ij} = 1 when i=j, and δ_{ij} = 0 when i≠j;
  μ = viscosity, dyn/cm;
  Δ = component of the rate of strain tensor.

The components of the *linearized* rate of strain tensor are linear functions of velocity vector gradients. For satisfying the boundary condition with spherical symmetry we need only know the radial normal stress τ_{rr}. It is found from the radial normal component of the rate of strain, which in spherical coordinates is given by

$$\Delta_{rr} = 2\,\partial v_r/\partial r \tag{31}$$

And so the boundary condition equation [29] is solved by $\tau_R = \tau_{rr}|_{r=R}$, which is readily evaluated; the boundary condition for a Newtonian liquid becomes

$$P_{out} + 2\sigma/R = P_{in} - 4\mu R'/R \tag{32}$$

For a linearly elastic solid, by definition the stress tensor components are linearly related to the components of the strain tensor[16]:

55

$$\tau_{ij} = \lambda(e_{11}+e_{22}+e_{33})\delta_{ij} + 2\mu e_{ij} \qquad [33]$$

where λ and μ are the Lamé constants;

e = small strain tensor component;

e_{11}, e_{22}, and e_{33} are the normal strain components.

(By longstanding convention, the second Lamé constant unfortunately is denoted by the same Greek letter as is the viscosity of a liquid.) Equation [33] does not appear at first to contain the hydrostatic pressure, but we can make the substitution[16]

$$\begin{aligned} P &= -B(e_{11}+e_{22}+e_{33}) \\ &= -(\lambda + 2)(e_{11}+e_{22}+e_{33}) \qquad [34] \end{aligned}$$

where B = bulk modulus, dyn/cm^2.

Equation [33] now becomes

$$\tau_{ij} = [-P - (2\mu/3)(e_{11}+e_{22}+e_{33})]\delta_{ij} + 2\mu e_{ij} \qquad [35]$$

The continuity equation tells us that in an *incompressible* system the sum of the normal strain components $(e_{11}+e_{22}+e_{33})$ is zero, so we can simplify the constitutive relation to

$$\tau_{ij} = -P\delta_{ij} + 2\mu e_{ij} \qquad [36]$$

56

In *linearized* elastic theory the strain tensor components are linear functions of displacement vector gradients. For this spherically symmetric system we need to obtain the radial normal stress from the radial normal strain, which in spherical coordinates is given by

$$e_{rr} = \partial u_r / \partial r \qquad [37]$$

And so the boundary condition again is solved by $\tau_R = \tau_{rr}|_{r=R}$. This radial normal stress component is given by

$$\tau_{rr}|_{r=R} = -P - 4\mu \, (R-R_E)/R \qquad [38]$$

at the bubble surface. Finally, let us replace the Lamé constant with the more familiar Young's modulus E. For an incompressible solid $\mu = E/3$. Our final expression for the linearized elastic boundary condition is therefore

$$P_{out} + 2\sigma /R = P_{in} - (4E/3)(R-R_E)/R \qquad [39]$$

Linearized elastic theory is valid for small deformations. At larger strains we require the nonlinear theory, in which expressions for the strain components are calculated from gradients in the displacement vector without discarding terms of order 2 and higher. The mathematics involved in computing our boundary condition for this kind of system are well beyond the scope of this report. Fortunately, the result has been published[17]:

57

$$\tau_{rr}|_{r=R} = -P - (1/6)E [5 - 4(R_E/R) - (R_E/R)^4] \qquad [40]$$

The boundary condition on the equation of motion for large elastic deformations is given by

$$P_{out} + 2\sigma/R = P_{in} - (1/6)E [5 - 4(R_E/R) - (R_E/R)^4] \qquad [41]$$

This boundary condition approaches the one for a linear elastic solid (equation [39]) in the limit as $R \to R_E$.

So, the appropriate boundary condition is substituted into the equation of motion (Equation [19]) and that equation is solved either analytically or numerically to yield a description of an oscillating gas bubble. To obtain the analytic solution it is necessary to assume linear elasticity when modelling oscillations in a solid, so Equation [39] must be used to calculate the elastic stress on the bubble wall arising from oscillations of the radius about its static value R_0. However, the nonlinear Equation [40] is used to compute the elastic stress imposed on the wall of the static bubble, i.e. the stress arising from the difference between R_0 and R_E. Thus, in the analytic solution we have a linear oscillatory stress superimposed on a nonlinear static stress. When using the Galerkin method the nonlinear Equation [40] is used for all calculations of elastic stress.

There is one potential complication when figuring the boundary condition for a vibrating bubble in an elastic solid. The following relations are true for the strain and elastic stress in the solid surrounding the bubble:

$$\text{for } R > R_E \quad e_{rr} < 0 \quad \text{and } \tau_{rr} < 0, \qquad [42a]$$

and
$$\text{for } R \leq R_E \quad e_{rr} = 0 \quad \text{and } \tau_{rr} = 0, \qquad [42b]$$

where R_E = bubble radius at which the medium surrounding the bubble is undeformed. (The strain and stress are negative when $R > R_E$ because of our arbitrary sign convention.) Equation [42] says that the bubble pushes against the solid when $R > R_E$, but doesn't pull on it when $R < R_E$; that is, the solid does not adhere to the bubble wall. Consequently, the boundary condition is discontinuous at $R = R_E$. If a bubble is made to oscillate in size such that its radius is greater than R_E during expansions and less than R_E during contractions, then its boundary condition is discontinuous in time. Describing such a system mathematically would present formidable challenges. We therefore limit ourselves to analyzing systems for which R is never less than R_E during vibration. Experimentally, if a bubble is formed by cavitation in a solid then $R_E = 0$ and the discontinuous boundary condition can never exist. If, on the other hand, the solid phase is formed by solidifying a liquid around a gas bubble that is at its equilibrium radius R_0 then we expect that $R_E = R_0$, and if the bubble radius is made to oscillate about R_0 (in response to sound waves, for instance) then the boundary condition is discontinuous in time.

D. <u>Results: Bubbles in a viscous liquid</u>

Using FORTRAN programs that implement the models discussed above, we have generated the graphs shown below. In all these graphs, we show the maximum bubble radius attained during an oscillation after the system is in a steady state mode. The

maximum value is given as a function of the driving frequency; the latter is expressed as a ratio of driving frequency to natural frequency of the bubble.

The expression 'Galerkin Method' in the graph headings refers to the program that implements the Keller equation (see above) for bubble oscillations. In this program the differential equation modeling heat flow across the bubble wall is solved numerically using the Galerkin spectral method. The expression 'Perturbation Method' refers to the program which implements Rayleigh's equation (with the addition of thermal and acoustic regarding damping terms as discussed above, and a natural frequency ω_0 for the bubble which depends on the driving frequency ω). The graphs are based on approximate analytic solutions proposed by Prosperetti[10]. These two methods are used for the case of a bubble in water driven by a sound wave with a small amplitude (0.3 atm). For the associated graphs, see Figures 8 and 9. Figures 10 and 11 are graphs for the case of a bubble in water driven by a sound wave with a larger amplitude (0.6 atm). For this larger amplitude, which we use as well for the last four figures, we use another program based on Rayleigh's equation without the enhancements described above. The program, which we refer to as the 'Simple Model', solves the differential equation using a very accurate numerical method. Use of a numerical solution makes unnecessary certain analytic approximations required in the perturbation approach. The greater numerical accuracy achieved allows the simple model to handle large driving amplitudes which lead to numerical instabilities using the perturbation theory approach.

Figure 8: Maximum Bubble Radius (rel. to R_0); Galerkin Method
Bubble in H_2O; $R_0 = 10 \mu m$ Driving Amplitude $= .3$ atm.
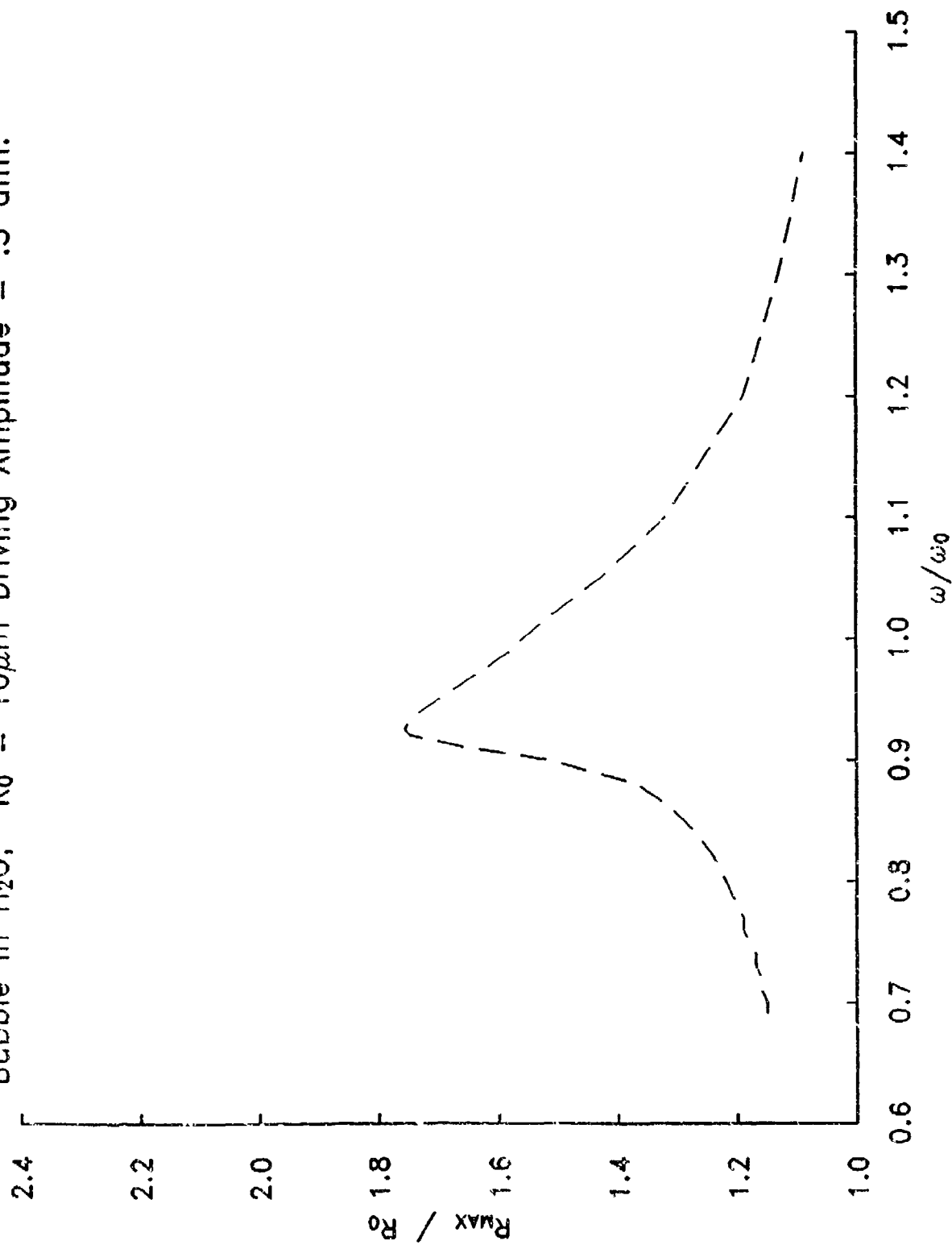
Figure 9: Maximum Bubble Radius (rel. to R_0); Perturbation Method
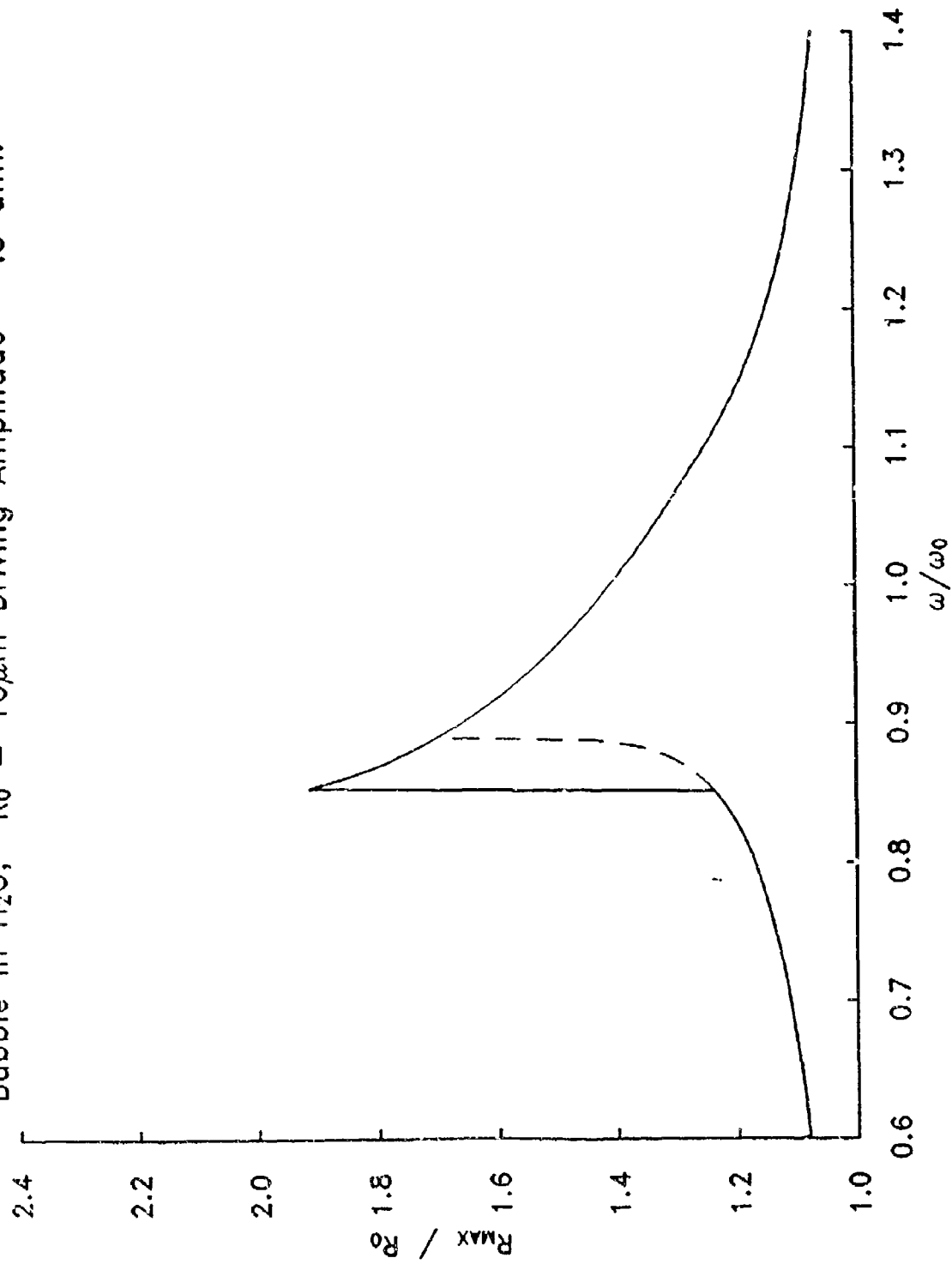Bubble in H_2O; $R_0 = 10\mu m$ Driving Amplitude $= .3$ atm.

Figure 10: Maximum Bubble Radius (rel. to R_0); Galerkin Method
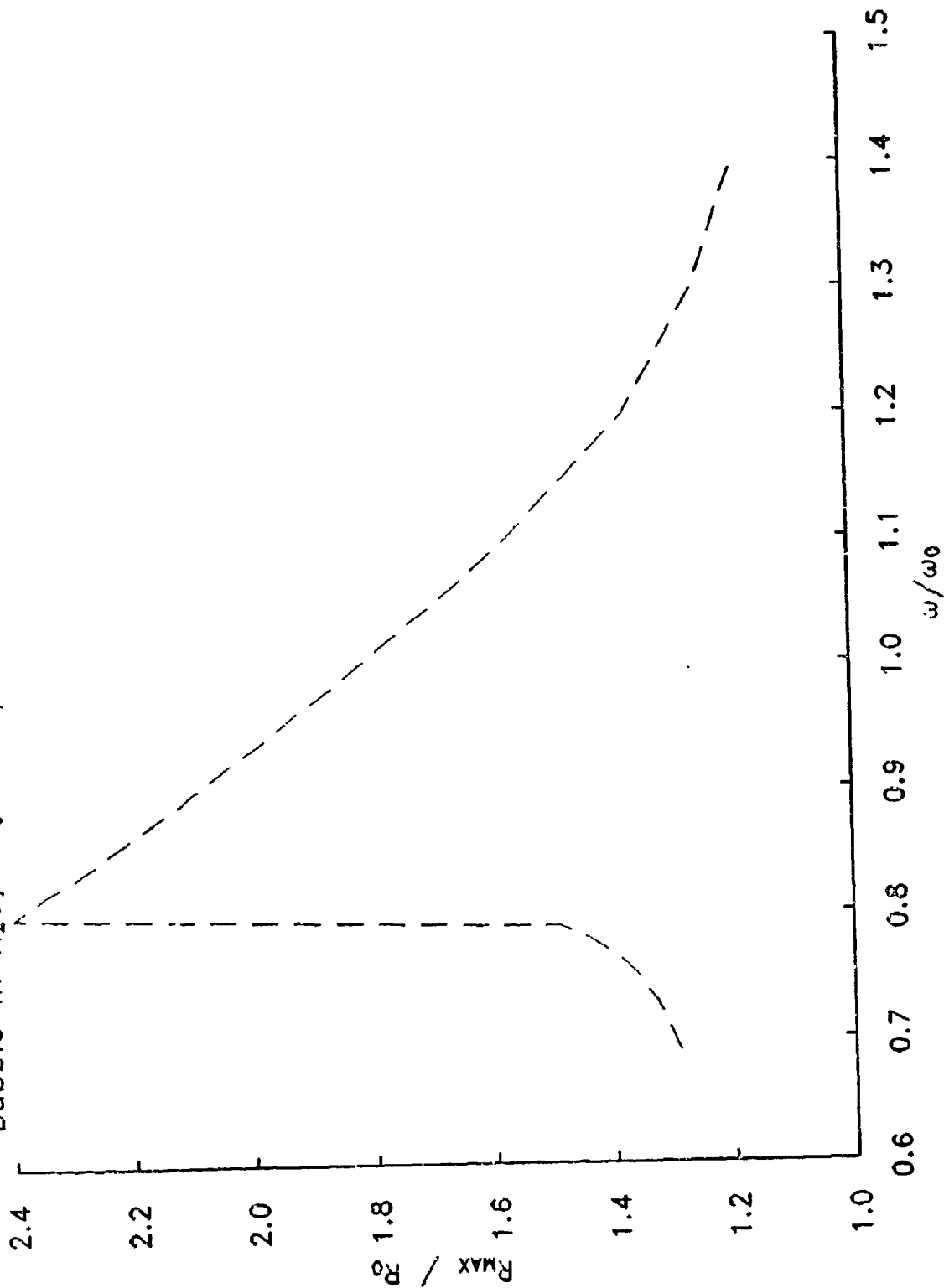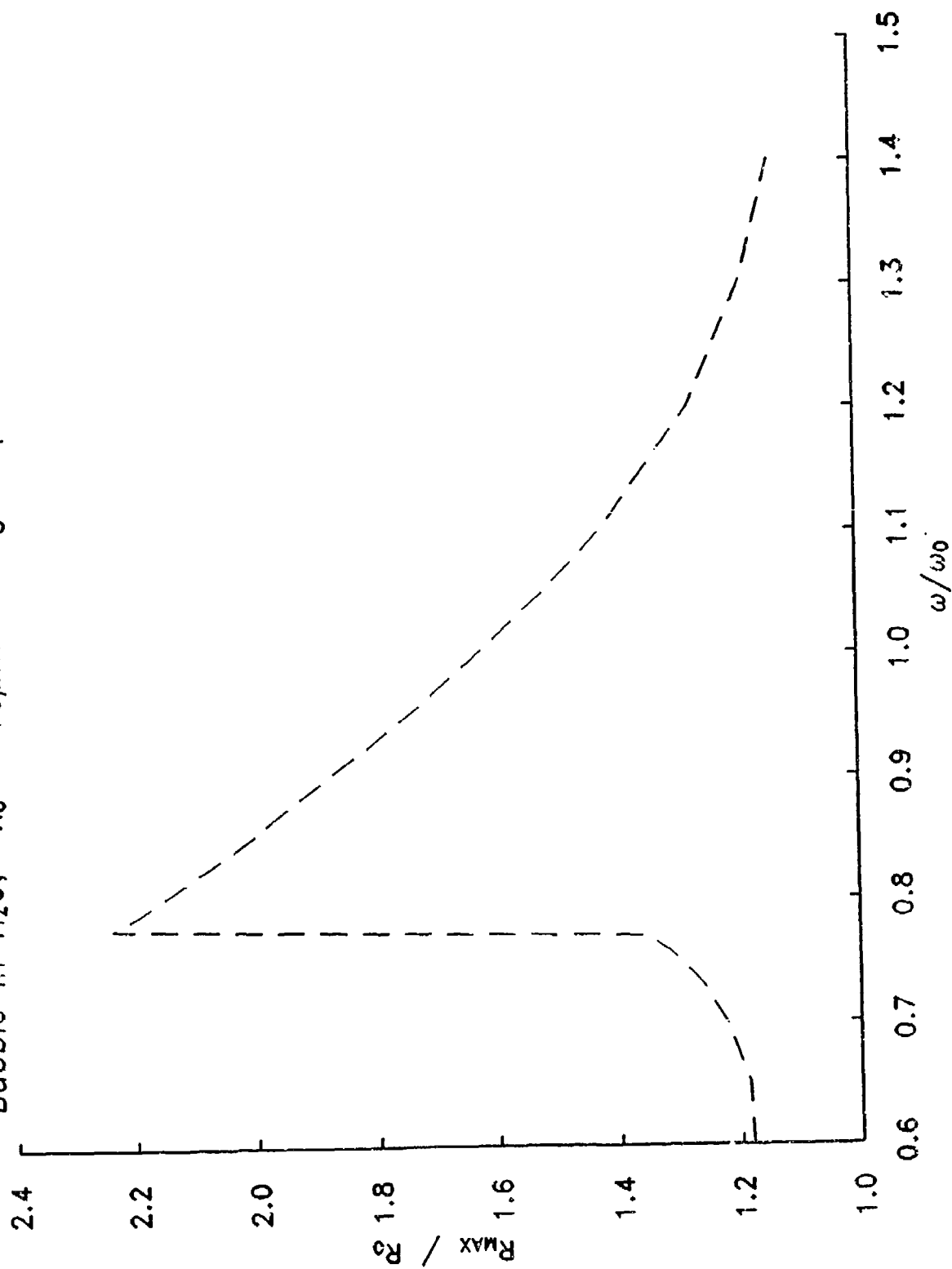Bubble in H_2O; R_0 = 10μm Driving Amplitude = .6 atm.

63

Figure 11: Maximum Bubble Radius (rel. to R_0); Simple Model Bubble in H_2O; R_0 = 10μm Driving Amplitude = .6 atm.

E. Results: Bubbles in an elastic solid

The last four figures apply to the case of an elastic solid with a shear modulus of $8 \cdot 10^5$ dyne/cm^2. This is a low value for the shear modulus and indicates a soft elastic solid. For example, this shear modulus would be typical of a fairly high-concentration polyacrylamide gel.[18] Figure 12 (Galerkin Method) and Figure 13 (Simple Model) describe the case of a bubble for which $R_0 = R_\sigma$ (recall that the latter is the radius at which there is no strain in the solid). This means that, at mechanical equilibrium, the solid is unstrained and the bubble wall is not subject to elastic stress. We use a common value of $10 \, \mu$m, because bubbles of this size are of interest. For Figure 14 (Galerkin Method) and Figure 15 (Simple Model), we consider the case of a bubble for which $R_0 > R_E$. We allow for large deformations; the nonlinear stress-strain relation is described by Equation 40. Here, $R_0 = 10 \, \mu$m, $R_E = 5 \, \mu$m.

In general, there are two stable solutions to both Rayleigh's and Keller's equation for values of the frequency ratio that lie in the resonance bands. The perturbation program will always find both these solutions since it has analytic expressions for them. The situation for the Galerkin program and the simple model program is more involved. The stable solution that is numerically calculated in these programs depends on the initial conditions; in general, starting with the bubble at rest and with radius R_0 leads to the solution with the smaller amplitude. Finding initial conditions that lead to another stable solution involves some numerical experimentation. For these differential equations only at most two stable solutions have been found to exist in any resonance band; however it is possible others exist. For the case described in Figure 13 we were

65

able to find such initial conditions (initial radius = $2 \cdot R_0$ cm, and initial velocity = R_0 cm/sec); therefc e we display both solutions. As the system is stiffened, either by increasing the shear modulus or by decreasing R_E, the two solutions may coalesce into a single one. One has to consider this possibility when one is unable to find more than one stable solution.

Figure 12: Maximum Bubble Radius (rel. to R_0); Galerkin Method, shear = 8e5, Bubble in Elastic Gel; $R_0 = R_E = 10\mu m$ Driving Amplitude = .6 atm.

67

Figure 13: Maximum Bubble Radius (rel. to R_0); Simple Model Bubble in Elastic Gel; $R_0 = R_\epsilon = 10\mu m$ Driving Amplitude = .6 atm.

68
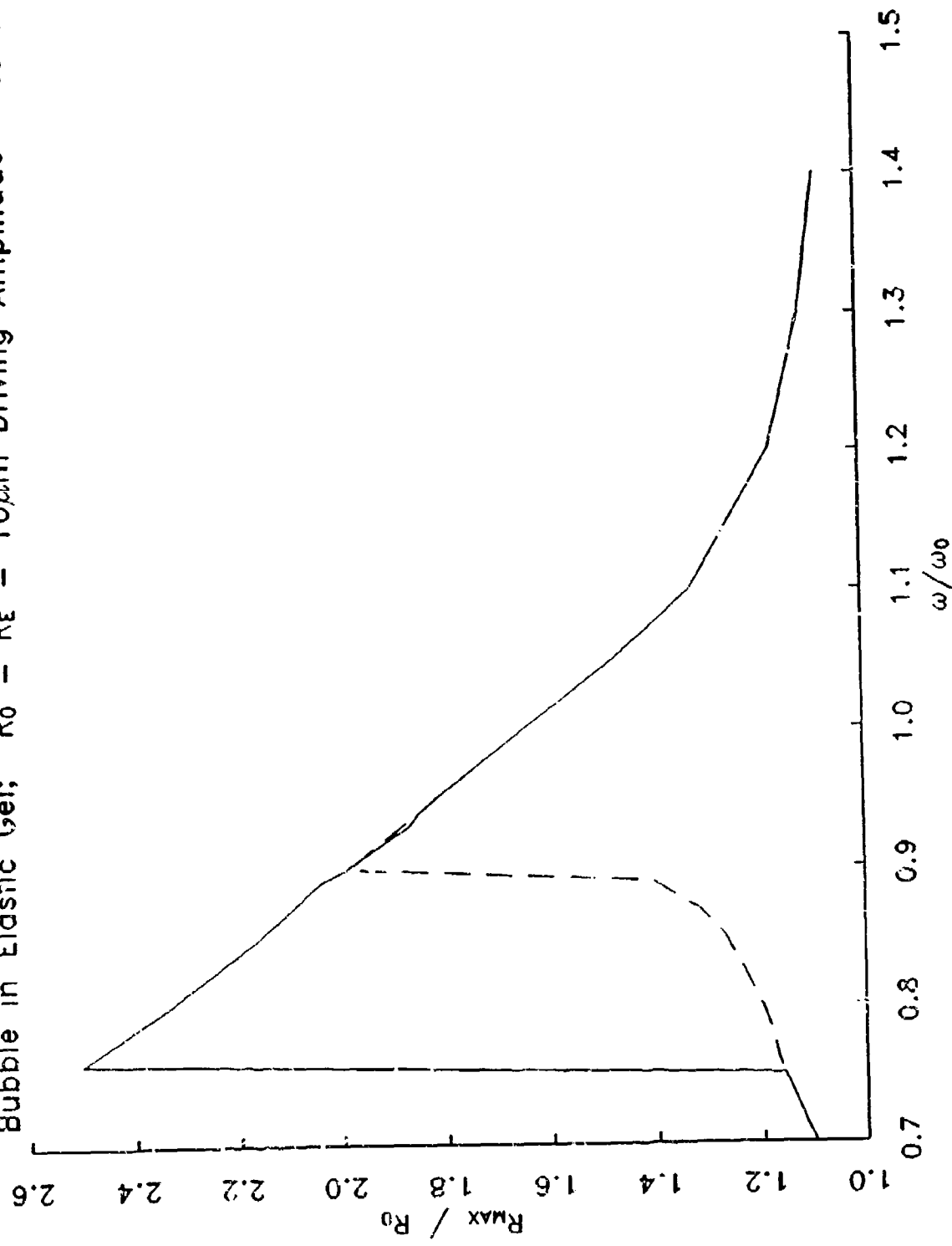
Figure 14: Maximum Bubble Radius (rel. to R_0); Galerkin Method. shear = 8e5, Bubble in Elastic Gel; $R_0 = 10\mu m$ $R_E = 5\mu m$ Driving Amplitude = .6 atm.
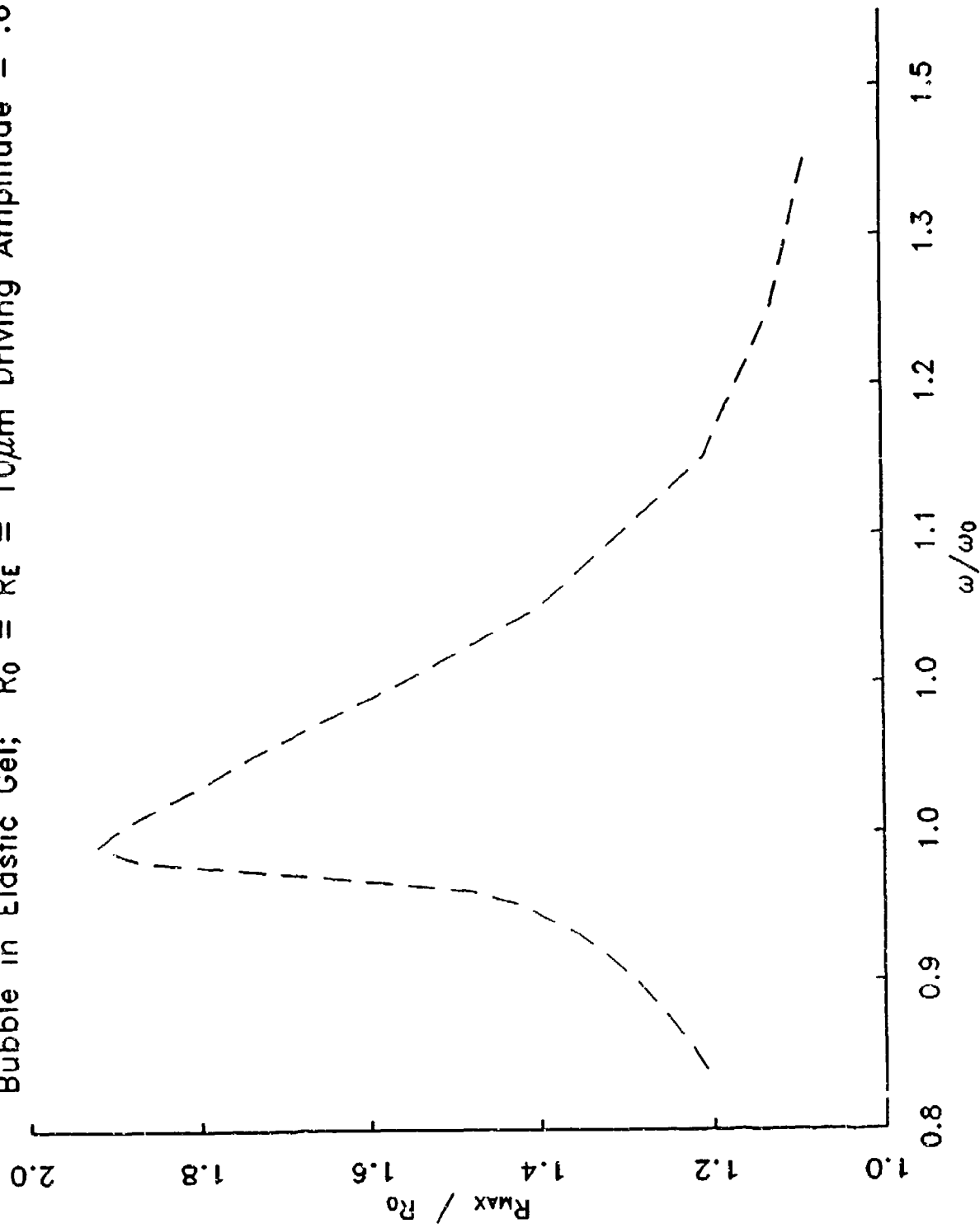
69
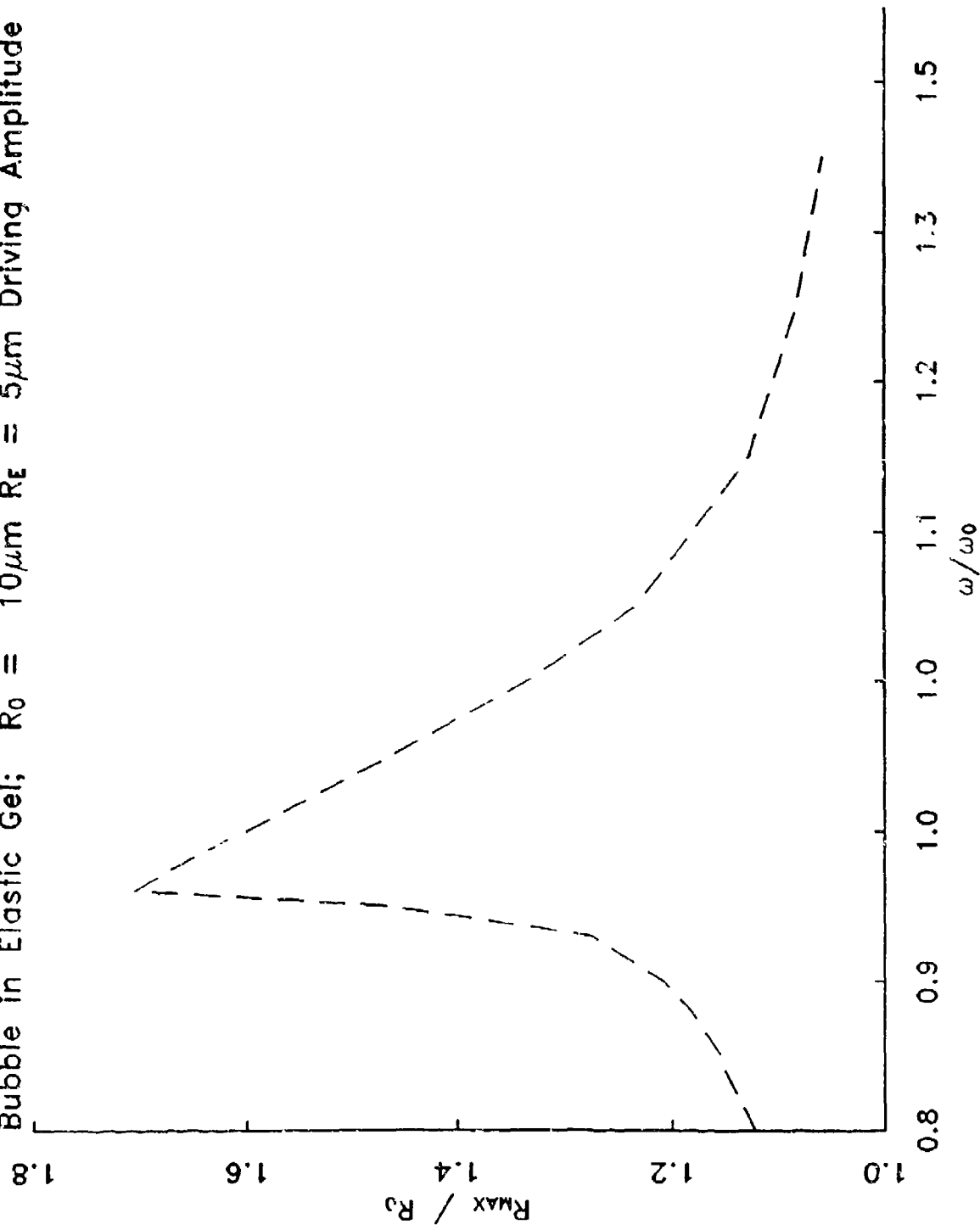
Figure 15: Maximum Bubble Radius (rel. to R_0); Simple Model, shear = 8e5, Bubble in Elastic Gel; R_0 = 10μm R_E = 5μm Driving Amplitude = .6 atm.

70
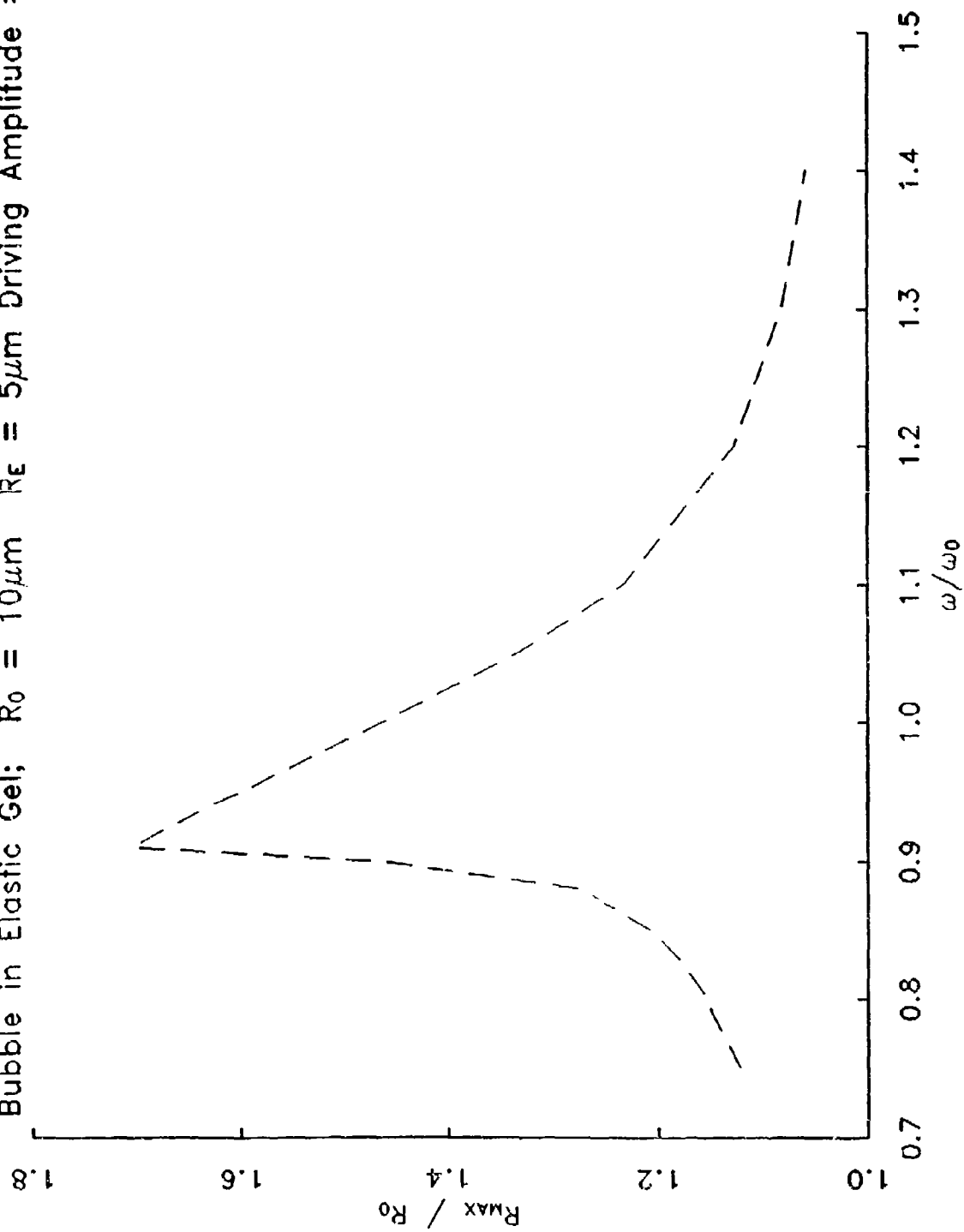
VIII. ESTIMATING THE SIGNAL/NOISE RATIO

We can use the models presented in section VII to estimate the ratio of [the sound pressure amplitude at the 2nd harmonic frequency radiated by a spherical bubble to the receiving transducer] to [the sound pressure amplitude at the fundamental frequency radiated by the transmitting transducer]. This tells us the "line loss" attendant with measuring a bubble. For instance, if P_{out} is one-twentieth of P_{in} then the line loss is 95% or 13 dB. If we assume that the bubble detector's overall frequency response is linear (that is, V_{out} is a linear function of V_{in}) then for this example V_{out} would be 13 dB below its maximum attainable value.

In section VI, 'Noise Measurements', we reported a relative noise level equal to the ratio of [the 2nd harmonic noise level] to [the maximum attainable level of the fundamental of the output signal]. Therefore, by inspection, we can estimate the S/N ratio of the system by dividing the line loss associated with a given bubble by the relative noise level as reported in section VI. In this section we discuss the estimated S/N ratio for single spherical bubbles of various sizes in water.

The line loss estimates were made using the analytic solution to the governing equations. The line loss is predicted to be only a weak function of the amplitude of the driving signal within the range of 0 to 0.5 atm sound pressure amplitude. The analytic solution is valid only at small amplitudes (i.e., small driving pressures), and the model yielded nonsensical results when it was extended to higher transmitted pressures,

71

precluding meaningful comment at this time about what happens with these stronger driving signals.

For a bubble in water the line loss is estimated to be ~31 dB for a 6 μm-diameter bubble and ~34.5 dB for a 0.9 μm-diameter bubble at transmitted sound pressure amplitudes of up to 0.5 atm.

Combining the predicted line loss with the noise measurements of section VI, we estimate the S/N ratio. At a setting of 3 V P-P on the 3325A signal generator the S/N ratio is estimated to be 6 dB for a 6 μm-diameter bubble and only -2.5 dB for a 0.9 μm-diameter bubble. This is uncomfortably low. There is no further improvement in the S/N ratio to be gained by signal averaging, because extensive signal averaging has been used already when obtaining the noise measurements. However, it is obvious from the sample data from section III that the noise level can be reduced by at least an order of magnitude by subtracting a judiciously chosen background measurement from the signal, which gives hope that the system may be sensitive enough to detect individual bubbles.

If the S/N ratio proves unacceptably low in practice, then for a remedy we may consider that the simulation results show that the signal level from a bubble is roughly proportional to the bubble diameter. Therefore, the S/N ratio could be increased, without replacing the existing electronic components with more linear components, by investigating larger bubbles. This approach would require that we replace the existing transducers with a pair designed for a lower frequency range, which would encompass the resonance frequencies of larger bubbles.

72

IX. CONCLUSIONS

The bubble detector has been redesigned and provided with appropriate software. It now has the potential to be of use.

Simulations of bubble oscillations have yielded important insights. These simulations, combined with measurements of the system noise, suggest that it may be difficult to detect a small ($\leq 6\,\mu$m diameter) bubble whose main resonance frequency is within the range over which the transducers are sensitive. A separate simulation of bubble size dynamics suggests that such small bubbles would be difficult to stabilize for the purpose of calibration. We also have learned via simulation that the signal strength increases linearly with bubble diameter and that bubble stability improves with size. Obviously, it may be advantageous to replace the present transducers with a pair that functions over a frequency range that encompasses the resonance frequencies of larger bubbles, and we are investigating that possibility. In the meantime, experiments will be undertaken to determine whether the existing system is capable of *ex vivo* detection of gas bubbles in dog spinal cords during and after decompression.

REFERENCES

1. Albin, G.W., P.B. Massell, and E.D. Thalmann. _Basic Operation of a Detector for Stationary Gas Bubbles_. Naval Medical Research Institute Technical Report 91-39, 1991.

2. Nyborg, W.L. Physical Principles of Ultrasound. _Ultrasound: Its Application in Medicine and Biology_, F.J. Fry, ed. New York: Elsevier, 1978.

3. Marquardt, D.W. "An Algorithm for Least-Squares Estimation of Nonlinear Parameters." _J. Soc. Ind. Appl. Math._ 11:431-441, 1963.

4. Flory, P.J., _Principles of Polymer Chemistry_. Cornell University Press, NY, 1953.

5. Harvey, E.N., D.K. Barnes, W.D. McElroy, A.H. Whitely, D.C. Pease, and K.W. Cooper. Bubble Formation in Animals; Physical Factors. _J. Cell. Comp. Physiol._ 24: 1-22, 1944.

6. Treybal, R.E. _Mass Transfer Operations_, McGraw-Hill Book Company, NY, 1980.

7. Reid, R.C. The properties of gases and liquids, their estimation and correlation. Reid, R.C. and T.K. Sherwood, eds. New York: McGraw-Hill, 1966.

8. Weathersby, P.K. and L.D. Homer. Solubility of Inert Gases in Biological Fluids and Tissues: A Review. _Undersea Biomed. Res._ 7:277-296, 1980.

9. Middleman, S. _Fundamentals of Polymer Processing_, New York: McGraw-Hill Book Company, 1977.

10. Prosperetti, A. Nonlinear Oscillations of Gas Bubbles in Liquids: Steady-State Solutions. _J. Acoust. Soc. Am._ 56:878-885, 1974.

11. Prosperetti, A. Thermal Effects and Damping Mechanisms in the Forced Radial Oscillations of Gas Bubbles in Liquids. J. Acoust. Soc. Am. 61:17-27, 1977.

12. Jackson, E. Atlee. Perspectives of Nonlinear Dynamics. Cambridge, United Kingdom: Press Cambridge, 1989.

13. Kamath, V. and A. Prosperetti. Numerical Integration Methods in Gas-Bubble Dynamics. J. Acoust. Soc. Am, 85:1538-1548, 1989.

14. Fletcher, C.A.J. Computational Galerkin Methods. New York: Springer-Verlag New York Inc., 1984.

15. Prosperetti, A., L. Crum, K. Commander. Nonlinear Bubble Dynamics. J. Acoust. Soc. Am, 83:502-514, 1988.

16. Achenback, J.D. Wave Propagation in Elastic Solids. New York: Elsevier, 1973.

17. Green, A.E. and W. Zerna. Theoretical Elasticity. London: Oxford University Press, 1954.

18. Nossal, R. Network Formation in Poltacrylamide Gels. Macromolecules 18:49-54, 1985.

APPENDIX

HP Basic Program to Control HP 3325A Signal Generator

and HP 3561A Signal Analyzer

APPENDIX: HP Basic Program to Control HP 3325A Signal Generator

and HP 3561A Signal Analyzer

```
10    ! THIS PROGRAM LISTS THE INITIAL SETTINGS FOR THE 3325A SIGNAL
20    ! GENERATOR, THE HP3561A SIGNAL ANALYZER, AND THEN OFFERS THE
30    ! OPPORTUNITY TO CHANGE SOME OF THESE DEFAULT SETTINGS. IT ALSO
40    ! TRIGGERS THE EXPERIMENT, EXTRACTS THE DATA FROM THE TIME BUFFER IN
50    ! THE 3561A, CONVERTS THE DATA TO AN AMPLITUDE-VERSUS-TIME SPECTRUM
60    ! (WHICH, BECAUSE OF THE NATURE OF THE EXPERIMENT IS ALSO AN
70    ! AMPLITUDE-VERSUS-FORCING FREQUENCY SPECTRUM), AVERAGES IT OVER A
80    ! USER-SELECTABLE NUMBER OF REPEAT MEASUREMENTS, SUBTRACTS THE
90    ! "BACKGROUND" (OR BASELINE) MEASUREMENT, STORES THE DATA
100   ! FOR LATER USE, AND PLOTS IT TO BOTH THE SCREEN AND A PRINTER.
110   !
120   OPTION BASE 1           ! MINIMUM NUMBER OF ELEMENTS IN AN ARRAY IS 1
130   PRINTER IS CRT          ! PRINTS TO SCREEN
140   RANDOMIZE               ! CHANGE SEED OF RANDOM NUMBER GENERATOR
150   !
160   INTEGER Zero(514)       ! THIS ARRAY TO BE USED TO FILL THE BUFFER
170   MAT Zero= (0)           ! AT I/O PATH '@Tag' WITH ZEROES
180                           ! IN BETWEEN TRACE DUMPS FROM THE SIG ANALYZER.
190   !
200   INTEGER Tag_field(350),Range,Rec_size
210   INTEGER Raw_data(30,1024) BUFFER
220   INTEGER Raw_raw_data(1024) BUFFER
230   INTEGER Raw_trace(401)                   ! FOR READING TRACE FROM BUFFER
240   INTEGER N,Limit,Sweeps,Sweep_back,Ii,I8
250   REAL Amplitude(512),Backgrnd(512),Negarea,Posarea
260   REAL Trace_data(401)    ! FOR CONVERTING BINARY TRACE DATA TO VOLTAGES
270   DIM Name$[15],File$[30]    ! FOR NAMING THE OUTPUT FILES
280   !
290   ASSIGN @Anz TO 711             ! OPEN THE I/O PATHS
300   ASSIGN @Siggen TO 717
310   ASSIGN @Header TO BUFFER [350];FORMAT OFF
320   ASSIGN @Time_buff TO BUFFER Raw_raw_data(*);FORMAT OFF
330   ASSIGN @Tag TO BUFFER [1028];FORMAT OFF
340   !
350   GOSUB Set_defaults
360   GOSUB Display_default
370   GOSUB Change_default
380   GOSUB Init_siggen
390   GOSUB Init_anz
400   !
410   !
420   BEEP (INT(RND*5127)+81),1
430   GOSUB How_many
440   GOSUB Index
450   !
460   Name$="\HPBLP\DATA\"
470   File$=Name$&"STRT"&VAL$(Istart)&".BCK"
480   BEEP (INT(RND*5127)+81),1
```

```
490  !
500  !        MEASURING BACKGROUND
510  !
520  INPUT "HIT 'ENTER' TO MAKE A BACKGROUND MEASUREMENT ",Dummy$
530  PRINT ""
540  PRINT "NOW COLLECTING THE BACKGROUND MEASUREMENT"
550  PRINT ""
560  N=0              ! INDEX N = 0 IF MAKING BACKGROUND MEASUREMENT,
570                   ! N = 1 IF COLLECTING REGULAR DATA
580  OUTPUT @Anz;"NAVG";Sweep_back     ! TRACE DATA ARE TIME AVERAGED OVER
590                                    ! "Sweep_back" NUMBER OF SWEEPS
600  OUTPUT @Anz;"SCAL"       ! 3561A SELF-CALIBRATION
610  WAIT 3               ! WAIT FOR 3561A SELF-CAL
620  OUTPUT @Anz;"STRT"       ! START TIME AVERAGE
630  FOR Ii=1 TO Sweep_back
640    GOSUB Trigger_system
650    GOSUB Read_data
660    WAIT Sweep_time     ! WAIT FOR SIG GEN TO CYCLE BACK
670  NEXT Ii
680  GOSUB Convert_and_sum
690  MAT Backgrnd= Amplitude
700  GOSUB Store_data
710  GOSUB Integrate
720  GOSUB Plot_data
730  DUMP GRAPHICS       ! PIXEL-BY-PIXEL DUMP OF SCREEN TO EXTERNAL PRINTER
740  !
750  CONTROL @Tag,3;1       ! MAKE SURE BUFFER POINT WRITER IS ON 1ST BYTE
760  OUTPUT @Tag;Zero(*)    ! FILL BUFFER WITH 514 INTEGER ZEROES
770  !
780  GOSUB Read_trace       ! DUMP TRACE FROM SIG ANALYZER TO BUFFER
790  GOSUB Scale_trace
800  GOSUB Plot_trace
810  DUMP GRAPHICS       ! PRINTING TRACE BY DUMPING SCREEN TO PRINTER
820  !
830  !        COLLECTING DATA
840  !
850  N=1              ! INDEX N = 0 IF MAKING BACKGROUND MEASUREMENT,
860                   ! N = 1 IF COLLECTING REGULAR DATA
870  OUTPUT @Anz;"NAVG";Sweeps  ! TRACE IS TIME-AVERAGED OVER "Sweeps"
880                   ! NUMBER OF SWEEPS
890  BEEP (INT(RND*5127)+81),1
900  !
910  PRINT ""
920  INPUT "HIT 'ENTER' TO START DATA COLLECTION",Dummy$
930  OUTPUT @Anz;"STRT"       ! START TIME AVERAGE
940  FOR I8=Istart TO (1000+Istart)        ! CAN DO UP TO 1000 COLLECTION CYCLES
950    File$=Name$&"AMP"&VAL$(I8)&".DAT"
960    PRINT ""
970    PRINT ""
980    BEEP (INT(RND*5127)+81,,1)
990    PRINT "NOW ON COLLECTION CYCLE NUMBER ";I8
1000   PRINT ""
1010   PRINT ""
1020   OUTPUT @Anz;"SCAL"       ! SIG AN CALIBRATES ITSELF
```

```
1030    WAIT 3                      ! WAIT FOR 3561A SELF-CAL
1040    OUTPUT @Anz;"STRT"         ! START TIME AVERAGE
1050    FOR Ii=1 TO Sweep
1060      GOSUB Trigger_system
1070      GOSUB Read_datay
1080      WAIT Sweep_time     ! WAIT FOR SIG GEN TO CYCLE BACK TO "START"
1090    NEXT Ii
1100    GOSUB Convert_and_sum
1110    !
1120    MAT Amplitude= Amplitude-Backgrnd    ! SUBTRACTING THE "BACKGROUND"
1130                                         ! MEASUREMENT BEFORE PROCEEDING
1140    GOSUB Store_data
1150    BEEP (INT(RND*5127)+81),1
1160    !
1170    GOSUB Integrate
1180    GOSUB Plot_data
1190    DUMP GRAPHICS
1200  !
1210  CONTROL @Tag,3;1
1220  OUTPUT @Tag;Zero(*)
1230  !
1240    GOSUB Read_trace
1250    GOSUB Scale_trace
1260    GOSUB Plot_trace
1270    DUMP GRAPHICS
1280    !
1290    PRINT "CYCLE COMPLETE; PAUSING BEFORE NEXT CYCLE"
1300    PRINT ""
1310    PRINT ""
1320    PRINT ""
1330    WAIT Waittime
1340  NEXT I8
1350  !
1360  ASSIGN @Path TO *         ! CLOSE THE I/O PATHS
1370  ASSIGN @Header TO *
1380  ASSIGN @Time_buff TO *
1390  ASSIGN @Tag TO *
1400  !
1410  STOP
1420  !
1430 Set_defaults:        !
1440  !                     SET DEFAULTS FOR PARAMETERS
1450  !
1460  !    DEFAULTS FOR SIGNAL GENERATOR
1470  !
1480 Sweep_start_f=1  !    START SWEEP AT 1 MHz
1490 Strt_sweep_unit$="MH"   ! MEGAHERTZ
1500  !
1510 Sweep_stop_f=10     !    STOP SWEEP AT 7
1520 Stop_sweep_unit$="MH"  ! MEGAHERTZ
1530  !
1540 Signal_amp=3        !    AMPLITUDE IS 3
1550 Sig_amp_unit$="VO"  !    VOLTS
1560  !
```

```
1570 !      SET DEFAULTS FOR ANALYZER
1580 !
1590 Start_freq_anz=1 !    START OF FREQUENCY SPAN IS AT 0.8
1600 Strt_f_anz_unit$="KHZ" ! KILOHERTZ
1610 !
1620 Span_freq_anz=2 !     SPAN OF FREQUENCIES IS 2
1630 Span_f_anz_unit$="KHZ" ! KILOHERTZ
1640 !
1650 Sweep_time=.4/Span_freq_anz      ! SWEEP TIME DEPENDS ON SPAN
1660 !
1670 Rcc_size=1
1680 !
1690 RETURN
1700 !
1710 Display_default:    !
1720 !                    SHOW CHANGEABLE DEFAULTS
1730 !
1740 PRINT "YOU ARE CONTROLLING THE HP 3325A SIG GEN, THE HP 3561A SIG AN,"
1750 PRINT "AND THE REST OF THE BUBBLE DETECTOR FROM THIS PC."
1760 PRINT ""
1770 PRINT ""
1780 PRINT "SOME OF THE DEFAULT SETTINGS ON THESE DELICATE INSTRUMENTS"
1790 PRINT "ARE HARD-CODED IN THIS IMMENSELY COMPLICATED PROGRAM, WHICH"
1800 PRINT "SHOULD BE TOUCHED ONLY BY HIGHLY TRAINED, AUTHORIZED PERSONNEL."
1810 PRINT "HOWEVER, OTHER SETTINGS CAN BE SELECTED EVEN BY AN"
1820 PRINT "IGNORANT LAYMAN LIKE YOURSELF."
1830 PRINT "FOR INSTANCE, THE START AND STOP FREQS FOR THE SWEEP,"
1840 PRINT "THE TIME TO COMPLETE A SWEEP, AND THE AMPLITUDE OF THE SWEEP"
1850 PRINT "CAN BE CHANGED. IN ADDITION, FOR THE ANALYZER, THE START FREQ"
1860 PRINT "AND FREQ SPAN CAN BE CHANGED."
1870 PRINT "NOT ONLY THAT, BUT YOU CAN SELECT HOW MANY SWEEPS WILL BE"
1880 PRINT "TIME-AVERAGED INTO EACH CYCLE, AND HOW LONG THE SYSTEM"
1890 PRINT "PAUSES BETWEEN CYCLES.  WHY, IT'S LIKE LIVING IN SPACE !!!"
1900 PRINT ""
1910 PRINT ""
1920 INPUT "PLEASE HIT THE ENTER KEY",Dummy$
1930 RETURN
1940 Display_setting:    !
1950 PRINT ""
1960 PRINT "THE SETTINGS FOR THESE INSTRUMENTS ARE."
1970 PRINT ""
1980 PRINT "FOR THE SIGNAL GENERATOR"
1990 PRINT ""
2000 PRINT " 1    SWEEP START FREQ =";Sweep_start_f;Strt_sweep_unit$
2010 PRINT " 2    SWEEP STOP FREQ =";Sweep_stop_f;Stop_sweep_unit$
2020 PRINT " 3    SWEEP TIME =";Sweep_time;"SECONDS"
2030 PRINT " 4    SIGNAL AMPLITUDE =";Signal_amp;Sig_amp_unit$
2040 PRINT ""
2050 PRINT "FOR THE ANALYZER"
2060 PRINT ""
2070 PRINT " 5    START FREQ =";Start_freq_anz;Strt_f_anz_unit$"
2080 PRINT " 6    FREQ SPAN =";Span_freq_anz;Span_f_anz_unit$
2090 PRINT ""
2100 RETURN
```

```
2110  !
2120  Change_default:       !
2130  !                     CHANGE ANY OF THE DEFAULTS?????
2140  !
2150  GOSUB Display_setting
2160  !
2170  First_question:       !
2180  !
2190  INPUT "DO YOU WISH TO CHANGE ANY OF THE SETTINGS (Y OR N) ?",Reply$
2200  SELECT Reply$
2210  CASE "N","n"
2220    RETURN
2230  CASE "Y","y"
2240    GOTO Make_changes
2250  CASE ELSE
2260    PRINT "PLEASE RESPOND WITH Y OR N"
2270    GOTO First_question
2280  END SELECT
2290  !
2300  Make_changes:       !
2310  !                   MAKE CHANGES IN SOME PARAMETERS
2320  !
2330  INPUT "PLEASE INDICATE (BY NUMBER) WHICH PARAMETER SHOULD BE CHANGED"
2340  SELECT
2350  !
2360  CASE 1
2370  !
2380    INPUT "PLEASE ENTER THE NEW SWEEP START FREQ",Sweep_start_f
2390    PRINT "WHAT ARE THE UNITS (CHOOSE FROM THE FOLLOWING)"
2400    PRINT ""
2410    PRINT "        HZ        HERTZ"
2420    PRINT "        KH        KILOHERTZ"
2430    INPUT "        MH        MEGAHERTZ",Strt_sweep_unit$
2440    GOTO Change_default
2450  !
2460  CASE 2
2470  !
2480    INPUT "PLEASE ENTER THE NEW SWEEP STOP FREQ",Sweep_stop_f
2490    PRINT "WHAT ARE THE UNITS (CHOOSE FROM THE FOLLOWING)"
2500    PRINT ""
2510    PRINT "        HZ        HERTZ"
2520    PRINT "        KH        KILOHERTZ"
2530    INPUT "        MH        MEGAHERTZ",Stop_sweep_unit$
2540    GOTO Change_default
2550  !
2560  CASE 3
2570  !
2580    INPUT "PLEASE ENTER THE NEW SWEEP TIME, IN SECONDS",Sweep_time
2590       ! IF CHANGE SWEEP TIME, CHANGE SPAN, TOO
2600    Span_freq_anz=.4/Sweep_time
2610    Span_f_anz_unit$="KHZ"
2620    GOTO Change_default
2630  !
2640  CASE 4
```

```
2650  !
2660  INPUT "PLEASE ENTER THE NEW SIGNAL AMPLITUDE",Signal_amp
2670  PRINT "WHAT ARE THE UNITS (CHOOSE FROM THE FOLLOWING)"
2680  PRINT ""
2690  PRINT "        VO        VOLTS"
2700  PRINT "        MV      MILLIVOLTS"
2710  PRINT "        VR      VOLTS RMS"
2720  INPUT "        MR        MV RMS",Sig_amp_unit$
2730  GOTO Change_default
2740  !
2750  CASE 5
2760  !
2770  INPUT "PLEASE ENTER THE NEW START FREQ FOR THE ANALYZER",Start_freq_anz
2780  PRINT "WHAT ARE THE UNITS (CHOOSE FROM THE FOLLOWING)"
2790  PRINT ""
2800  PRINT "        HZ        HERTZ"
2810  PRINT "        KHZ      KILOHERTZ"
2820  INPUT "        MHZ       MEGAHERTZ",Strt_f_anz_unit$
2830  GOTO Change_default
2840  !
2850  CASE 6
2860  !
2870  INPUT "PLEASE ENTER THE NEW SPAN FREQ FOR THE ANALYZER",Span_freq_anz
2880  PRINT "WHAT ARE THE UNITS (CHOOSE FROM THE FOLLOWING)"
2890  PRINT ""
2900  PRINT "        HZ        HERTZ"
2910  PRINT "        KHZ      KILOHERTZ"
2920  INPUT "        MHZ       MEGAHERTZ",Span_f_anz_unit$
2930  !   IF CHANGE SPAN, CHANGE SWEEP TIME, TOO:
2940  IF Span_f_anz_unit$="HZ" THEN Sweep_time=400/Span_freq_anz
2950  IF Span_f_anz_unit$="KHZ" THEN Sweep_time=.4/Span_freq_anz
2960  IF Span_f_anz_unit$="MHZ" THEN Sweep_time=.0004/Span_freq_anz
2970  GOTO Change_default
2980  !
2990  CASE ELSE
3000  !
3010  PRINT "PLEASE CHOOSE AN INTEGER FROM 1 TO 6"
3020  GOTO Change_default
3030  !
3040  END SELECT
3050  RETURN
3060  !
3070  Init_siggen:    !
3080  !               INITIALIZE THE SIGNAL GENERATOR
3090  !
3100  OUTPUT @Siggen;"ST";Sweep_start_f;Strt_sweep_unit$
3110  OUTPUT @Siggen;"SP";Sweep_stop_f;Stop_sweep_unit$
3120  OUTPUT @Siggen;"TI";Sweep_time;"SE"
3130  OUTPUT @Siggen;"AM";Signal_amp;Sig_amp_unit$
3140  OUTPUT @Siggen;"RF2"
3150  !
3160  RETURN
3170  !
3180  Init_anz:      !
```

```
3190 !                      INITIALIZE THE ANALYZER
3200 ! SEE HP MANUALS FOR THE MEANINGS OF THE FOLLOWING HP-IB MNEMONICS
3210 OUTPUT @Anz;"TACM"      ! TIME CAPTURE MODEL
3220 OUTPUT @Anz;"SF";Start_freq_anz;Strt_f_anz_unit$
3230 OUTPUT @Anz;"SP";Span_freq_anz;Span_f_anz_unit$
3240 OUTPUT @Anz;"AVTI"      ! USING TIME AVERAGING ON THE 3561A
3250 OUTPUT @Anz;"FLAT"      ! CHOOSE FLATTOP WINDOWING
3260 OUTPUT @Anz;"SLTA"           ! DEFINE TRACE 'A'
3270 OUTPUT @Anz;"VSFS.3MVRM"       ! SET VERTICAL SCALE FOR TRACE
3280                            ! DISPLAY ON FRONT PANEL OF 3561A
3290 OUTPUT @Anz;"VSLI"           ! LINEAR VERTICAL SCALE
3300 OUTPUT @Anz;"MAG"             ! CHOOSE MAGNITUDE DISPLAYED
3310 OUTPUT @Anz;"SLTB"          ! DEFINE TRACE 'B'
3320 OUTPUT @Anz;"TIRE"           ! REAL TIME DISPLAY
3330 OUTPUT @Anz;"TBNR1REC"        ! ONE TIME RECORD AT A TIME IN THE BUFFER
3340 OUTPUT @Anz;"TRGR"
3350 OUTPUT @Anz;"EXT"
3360 OUTPUT @Anz;"SLOPNEG"    ! EXTERNAL TRIGGER; TRIGGERED BY NEGATIVE SLOPE
3370 !
3380 PRINT "WAITING WHILE ANALYZER IS BEING INITIALIZED"
3390 WAIT 5
3400 !
3410    ! DO ONE AUTORANGE ON THE 3561A SIGNAL ANALYZER:
3420 OUTPUT @Siggen;"SC"          ! START CONTINUOUS RUN ON 3325A
3430 WAIT .5
3440 OUTPUT @Anz;"SARG"           ! DO ONE AUTORANGE ONLY
3450 PRINT ""
3460 PRINT "WAITING FOR SIGNAL ANALYZER TO AUTORANGE"
3470 PRINT ""
3480 !
3490 WAIT 8          ! WAIT FOR COMPLETION OF AUTORANGING
3500 OUTPUT @Anz;"SCAP"    ! INTO TIME CAPTURE MODE
3510 WAIT Sweep_time+.5
3520 OUTPUT @Anz;"DTBB"    ! DUMPING TIME BUFFER IN BINARY TO PC
3530 TRANSFER @Anz TO @Header;COUNT 350,WAIT
3540 CONTROL @Header,5;35        ! GET RANGE FROM HEADER
3550 ENTER @Header;Range
3560 Factor=4/3*10^((Range+4.812)/20)/32768 ! FOR CONVERTING TIME BUFFER DATA
3570                                        ! FROM BINARY TO VOLTAGE
3580 !
3590 OUTPUT @Anz;"ACAL OFF"   ! DISABLES AUTOCALIBRATION OF 3561A
3600 OUTPUT @Anz;"ARNG OFF"     ! DISABLES AUTORANGING OF 3561A
3610 OUTPUT @Siggen;"SS"     ! RESETS 3325A SIG GEN
3620 RETURN
3630 !
3640 How_many:     ! HOW MANY SWEEPS TO PERFORM PER CYCLE
3650               ! AND HOW LONG BETWEEN CYCLES
3660 !
3670 PRINT ""
3680 PRINT ""
3690 INPUT "HOW MANY SWEEPS PER CYCLE ...
              ...DURING REGULAR DATA COLLECTION (1 TO 20) ?",Sweeps
3700 IF Sweeps>20 OR Sweeps<1 THEN How_many
3710 !
```

```
3720 How_many_back:  !  HOW MANY SWEEPS DURING BKGD MEASUREMENT
3730 INPUT "HOW MANY SWEEPS PER CYCLE DURING ...
                      ...BACKGROUND MEASUREMENT (1 TO 30) ?",Sweep_back
3740 IF Sweep_back>30 OR Sweep_back<1 THEN How_many_back
3750 !
3760 How_long:      !
3770 INPUT "HOW LONG (IN SECONDS) BETWEEN CYCLES ?",Waittime
3780 IF Waittime<10 THEN
3790    PRINT "TOO SHORT AN INTERVAL; CHOOSE A TIME OF AT LEAST 10 SEC"
3800    GOTO How_long
3810 END IF
3820 !
3830 PRINT ""
3840 RETURN
3850 !
3860 Index:          !
3870 INPUT "THE DATA FILES WILL BE NUMBERED, STARTING WITH NUMBER --",Istart)
3880 PRINT ""
3890 RETURN
3900 !
3910 Trigger_system:  !   BEGIN THE DATA COLLECTION
3920 !
3930 OUTPUT @Anz;"SCAP"      ! ANALYZER IN START CAPTURE MODE
3940 WAIT Sweep_time+.5
3950 OUTPUT @Siggen;"SSSS"    ! THE FIRST "SS" RESETS THE SIGNAL GEN
3960                          ! AND THE SECOND STARTS THE SWEEP
3970 WAIT Sweep_time       ! WAIT FOR SWEEP TO FINISH BEFORE
3980                       ! TRYING TO READ TIME BUFFER
3990 RETURN
4000 !
4010 Read_data:      !   GET BUFFERED DATA FROM THE ANALYZER
4020 !
4030 IF N=0 THEN Limit=Sweep_back     ! N=0 MEANS BKGD BEING MEASURED
4040 IF N=1 THEN Limit=Sweeps        ! N=1 MEANS REGULAR DATA BEING COLLECTED?
4050 PRINT "    ON SWEEP ";Ii;" OF ";Limit
4060 PRINT ""
4070 !
4080 OUTPUT @Anz;"DTBB"
4090 New_read:        !"
4100 CONTROL @Header,3;1
4110 CONTROL @Time_buff,3;1
4120 TRANSFER @Anz TO @Header;COUNT 350,WAIT
4130 TRANSFER @Anz TO @Time_buff;COUNT 2048,WAIT
4140 MAT Raw_data(Ii,*)= Raw_raw_data
4150 RETURN
4160 !
4170 !
4180 Convert_and_sum:  ! GET AN AVERAGE FOR THE DATA OVER SEVERAL SWEEPS
4190 !
4200 PRINT ""
4210 IF N=0 THEN                  ! N=0 MEANS BKGD BEING MEASURED
4220    Limit=Sweep_back
4230    PRINT "NOW AVERAGING OVER THE ";Limit;" SWEEPS"
4240 END IF
```

```
4250  IF N=1 THEN            ! N=1 MEANS REGULAR DATA BEING COLLECTED
4260    Limit=Sweeps
4270  PRINT "NOW AVERAGING OVER THE ";Limit;" SWEEPS AND SUBTRACTING BACKGROUND"
4280  END IF
4290  !
4300  FOR J=1 TO 512
4310    Amplitude(J)= 0
4320    FOR Ii=1 TO Limit
4330    !    CONVERT TO AMPLITUDE AND DO TIME AVERAGING SIMULTANEOUSLY
4340      Amplitude(J)=SQRT(Raw_data(Ii,2*J-1)^2+ Raw_data(Ii,2*J)^2)+Amplitude(J)
4350    NEXT Ii
4360  NEXT J
4370  MAT Amplitude = Amplitude*(Factor/Limit))
4380  RETURN
4390  !
4400  !
4410  Store_data:     ! STORE AMPLITUDE SPECTRUM AFTER SUBTRACTING BACKGROUND
4420  !
4430  CREATE BDAT File$,512,8
4440  ASSIGN @Path TO File$
4450  OUTPUT @Path;Amplitude(*)
4460  !
4470  RETURN
4480  !
4490  Integrate:           ! FIND AREA UNDER VOLTAGE AMPLITUDE SPECTRUM;
4500                       ! SEPARATE POSITIVE AND NEGATIVE CONTRIBUTIONS TO TOTAL AREA
4510  Area=0
4520  Posarea=0
4530  Negarea=0
4540  FOR Int=1 TO 512
4550    Area=(Amplitude(Int)+Amplitude(Int+1))+Area
4560    IF Amplitude(Int)>=0 AND Amplitude(Int+1)>=0 THEN
4570      Posarea=Posarea+Amplitude(Int)+Amplitude(Int+1)
4580    ELSE
4590      IF Amplitude(Int)<=0 AND Amplitude(Int+1)<=0 THEN
4600        Negarea=Negarea+Amplitude(Int)+Amplitude(Int+1)
4610      ELSE
4620        IF Amplitude(Int)>0 AND Amplitude(Int+1)<0 THEN
4630          Posarea=Amplitude(Int)*Amplitude(Int)/(Amplitude(Int)-Amplitude(Int+1))+Posarea
4640          Negarea=Amplitude(Int+1)*(1+Amplitude(Int)/(Amplitude(Int+1)-Amplitude(Int)))+Negarea
4650        ELSE
4660          IF Amplitude(Int)<0 AND Amplitude(Int+1)>0 THEN
4670            Posarea=Amplitude(Int+1)*(1+Amplitude(Int)/(Amplitude(Int+1)-Amplitude(Int)))+Posarea
4680            Negarea=Amplitude(Int)*Amplitude(Int)/(Amplitude(Int)-Amplitude(Int+1))+Negarea
4690          END IF
4700        END IF
4710      END IF
4720    END IF
4730  NEXT Int
4740  !
4750  IF Strt_sweep_unit$="HZ" THEN Startf=Sweep_start_f/1.E+6
4760  IF Strt_sweep_unit$="KH" THEN Startf=Sweep_start_f/1.E+3
4770  IF Strt_sweep_unit$="MH" THEN Startf=Sweep_start_f
4780  IF Stop_sweep_unit$="HZ" THEN Stopf=Sweep_stop_f/1.E+6
```

```
4790  IF Stop_sweep_unit$ "KH" THEN Stopf = Sweep_stop_f 1 E + 3
4800  IF Stop_sweep_unit$ "MH" THEN Stopf = Sweep_stop_f
4810  !
4820  Area = Area*.5*(Stopf-Startf)*1.E + 6 512            ' CONVERTS TO uV MHz
4830  Posarea = Posarea*.5*(Stopf-Startf)*1 E + 6 512      ' CONVERTS TO uV MHz
4840  Negarea = Negarea*.5*(Stopf-Startf)*1 E + 6 512      ' CONVERTS TO uV MHz
4850  !
4860  RETURN
4870  !
4880  Plot_data        ' DISPLAY THE DATA ON SCREEN
4890  !
4900  CLEAR SCREEN   ' ALPHA DISPLAY RETAINED AS GRAPHICS DISPLAY IS CALLED UP
4910  GCLE   R
4920  GINIT
4930  !
4940    ! DETERMINE HOW FAR THE Y AXIS SHOULD EXTEND
4950  REAL Absamp(512)
4960  MAT Absamp = ABS(Amplitude)    ' CONVERT Amplitude MATRIX TO MAGNITUDES
4970  Maxi = MAX(Absamp(*))          ' DETERMINE MAGNITUDE OF LARGEST Y VALUE
4980  Ylim = 100*(INT(Maxi*1.E + 4) + 1) ! MAX VALUE ON Y AXIS, PLOT IN MICROVOLTS
4990  !
5000  IF N = 0 THEN                  ! LABEL THE PLOT AND THE AXIS
5010    MOVE 26,95
5020    LABEL "BACKGROUND @ "&TIMES(TIMEDATE)&" "&DATES(TIMEDATE)
5030  ELSE                ! N = 1; SIGNAL BEING MEASURED
5040    MOVE 50,95
5050    LABEL "SIGNAL @ "&TIMES(TIMEDATE)
5060  END IF
5070  !
5080  MOVE 9,75
5090  Label$ = "Voltage"
5100  FOR I = 1 TO 7
5110    LABEL Label$[i,I]
5120  NEXT I
5130  !
5140  MOVE 13,80
5150  Label$ = "Amplitude"
5160  FOR I = 1 TO 9
5170    LABEL Label$[i,I]
5180  NEXT I
5190  !
5200  MOVE 41,17
5210  LABEL "Forcing Frequency (MHz)"
5220  MOVE 18,89
5230  LABEL VAL$(Ylim)&" uV"
5240  MOVE 22.58
5250  LABEL "0 uV"
5260  MOVE 15,29
5270  LABEL VAL$(-Ylim)&" uV"
5280  MOVE 36,23
5290  !
5300  IF Strt_sweep_unit$ = "HZ" THEN LABEL VAL$(Sweep_start_f/1.E+6)
5310  IF Strt_sweep_unit$ = "KH" THEN LABEL VAL$(Sweep_start_f/1.E+3)
5320  IF Strt_sweep_unit$ = "MH" THEN LABEL VAL$(Sweep_start_f)
```

```
5330  MOVE 106,23
5340  IF Stop_sweep_unit$="HZ" THEN LABEL VAL$(Sweep_stop_f/1.E+6)
5350  IF Stop_sweep_unit$="KH" THEN LABEL VAL$(Sweep_stop_f/1.E+3)
5360  IF Stop_sweep_unit$="MH" THEN LABEL VAL$(Sweep_stop_f)
5370  !
5380  MOVE 6,9
5390  LABEL USING "17A,S6D.2D,15A";"POSITIVE AREA IS ",Posarea," microvolts-MHz"
5400  MOVE 6,4
5410  LABEL USING "17A,S6D.2D,15A";"NEGATIVE AREA IS ",Negarea," microvolts-MHz"
5420  !
5430  VIEWPORT 38,108,30,90          ! POSITION THE GRAPH ON THE CRT
5440  WINDOW 0,Sweep_time,(-Ylim/1.E+6),(Ylim/1.E+6)   ! SIZE THE AXES
5450  AXES Sweep_time/10,(Ylim/1.E+6)/10,0,0          ! ADD TICK MARKS
5460  !
5470  PEN 1
5480  Dx=(Sweep_time/(Rec_size))/512
5490  X=0
5500  MOVE 0,Amplitude(1)
5510  FOR I=1 TO 512
5520    DRAW X,Amplitude(I)           ! PLOT THE DATA
5530    X=X+Dx
5540  NEXT I
5550  RETURN
5560  !
5570  Read_trace:      ! READ THE MAGNITUDE TRACE FROM THE 3561A,
5580                   ! MAGNITUDE HAS BEEN TIME-AVERAGED ON THE 3561A.
5590  OUTPUT @Anz;"SLTA"      ! ACTIVATE TRACE A, THE MAGNITUDE TRACE
5600  OUTPUT @Anz;"DSTB"            ! DUMP ACTIVE TRACE AND HEADER DATA
5610  TRANSFER @Anz TO @Tag;END,WAIT   ! TRANSFER TO BUFFER ON PC
5620  CONTROL @Tag,5;5         ! POSITION THE BUFFER POINT READER TO BYTE 5
5630  ENTER @Tag;Raw_trace(*)    ! READ THE DATA FROM THE TRACE INTO AN ARRAY
5640  !
5650  RETURN
5660  !
5670  Scale_trace:      ! CONVERT BINARY DATA TO VOLTAGE
5680  FOR It=1 TO 401
5690    Trace_data(It)=10.^(Raw_trace(It)*.005/20.)   ! CONVERTS TO VOLTAGE
5700  NEXT It
5710  RETURN
5720  !
5730  Plot_trace:      ! DISPLAY THE TRACE FROM THE 3561A ON SCREEN
5740  !
5750  CLEAR SCREEN   ! ALPHA DISPLAY RETAINED AS GRAPHICS DISPLAY IS CALLED UP
5760  GCLEAR
5770  GINIT
5780  !
5790  Maxi=MAX(Trace_data(*))
5800  Ymax=100*(INT(Maxi*1.E+4)+1) ! MAX VALUE OF Y; PLOTTING IN MICROVOLTS
5810    ! DETERMINE HOW FAR THE Y-AXIS SHOULD EXTEND:
5820  Ylim=Ymax
5830  !
5840  IF N=0 THEN                ! LABEL THE PLOT AND THE AXES
5850    MOVE 47,95
5860    LABEL "BACKGROUND TRACE"
```

```
5870  ELSE              ! N = 1; SIGNAL BEING MEASURED
5880    MOVE 50,94
5890    LABEL "SIGNAL TRACE"
5900  END IF
5910  !
5920  MOVE 9,75
5930  Label$="Voltage"
5940  FOR I=1 TO 7
5950    LABEL Label$[I,I]
5960  NEXT I
5970  !
5980  MOVE 13,80
5990  Label$="Amplitude"
6000  FOR I=1 TO 9
6010    LABEL Label$[I,I]
6020  NEXT I
6030  !
6040  MOVE 42,17
6050  LABEL "Offset Frequency (kHz)"
6060  MOVE 18,89
6070  LABEL VAL$(Ymax)&" uV"
6080  MOVE 22,29
6090  LABEL "0 uV"
6100  !
6110  IF Strt_f_anz_unit$="HZ" THEN Start_freq_anz=Start_freq_anz/1.E+3
6120  IF Strt_f_anz_unit$="MHZ" THEN Start_freq_anz=Start_freq_anz*1.E+3
6130  IF Span_f_anz_unit$="HZ" THEN Span_freq_anz=Span_freq_anz/1.E+3
6140  IF Span_f_anz_unit$="MHZ" THEN Span_freq_anz=Span_freq_anz*1.E+3
6150  !
6160  MOVE 36,23
6170  LABEL VAL$(Start_freq_anz)
6180  MOVE 106,23
6190  LABEL VAL$(Start_freq_anz+Span_freq_anz)
6200  !
6210  VIEWPORT 38,108,30,90              ! POSITION THE GRAPH ON THE CRT
6220  WINDOW 0,Span_freq_anz,0,(Ylim/1.E+6)   ! SIZE THE AXES
6230  AXES Span_freq_anz/10,(Ylim/1.E+6)/10,0,0       ! ADD TICK MARKS
6240  !
6250  PEN 1
6260  Dx=Span_freq_anz/400
6270  X=0
6280  MOVE 0,Trace_data(1)
6290  FOR It=1 TO 401
6300    DRAW X,Trace_data(It)           ! PLOT THE DATA
6310    X=X+Dx
6320  NEXT It
6330  RETURN
6340  !
6350  END
```